# Site-Selective Incorporation of Zerovalent Platinum and Palladium Fragments into Diplatinum Centers Supported by a Triphosphine Ligand

Tomoaki Tanase,*,† Hirokazu Ukaji, Hiroyuki Takahata, Hirotaka Toda, Toshiaki Igoshi, and Yasuhiro Yamamoto*

*Department of Chemistry, Faculty of Science, Toho University, Miyama 2-2-1, Funabashi, Chiba 274, Japan*

*Received August 15, 1997*

Reaction of $[Pt_2(RNC)_6](PF_6)_2$ (R = 2,6-xylyl (Xyl) (**a**) and 2,4,6-mesityl (Mes) (**b**)) with 2 equiv of bis((diphenylphosphino)methyl)phenylphosphine (dpmp) afforded a mixture of isomeric diplatinum complexes, *syn*-$[Pt_2(\mu\text{-dpmp})_2(RNC)_2](PF_6)_2$ (**1**) and *anti*-$[Pt_2(\mu\text{-dpmp})_2(RNC)_2](PF_6)_2$ (**2**), which were purified by cycles of recrystallization and were characterized by X-ray crystallography. Complexes **1** and **2** consist of a diplatinum core (Pt−Pt = 2.7094(8) Å (**1a**) and 2.683(2) Å (**2a**)) asymmetrically bridged by two dpmp ligands. The central phosphorus atoms of the dpmp ligands coordinate to the same metal center in the *syn*-dimer (**1**) and to different metal centers in the *anti*-dimer (**2**). Complexes **1** and **2** were fluxional in solution through symmetrical structures of *syn*-**1′** and *anti*-**2′**, respectively, in which two terminal phosphine units are uncoordinated. At reflux in $CH_3CN$ or by treatment with $[Cu(CH_3CN)_4](PF_6)$, complexes **1a** and **2a** lost one isocyanide molecule to be transformed into *syn*-$[Pt_2(\mu\text{-dpmp})_2(XylNC)](PF_6)_2$ (**3**, Pt−Pt = 2.6834(8) Å) and *anti*-$[Pt_2(\mu\text{-dpmp})_2(XylNC)](PF_6)_2$ (**4**, Pt−Pt = 2.7150(7) Å), respectively. Reactions of the *syn*-dimer (**1**) with $[M_3(XylNC)_6]$ readily afforded the linearly ordered trinuclear clusters, *linear*-$[Pt_2M(\mu\text{-dpmp})_2(XylNC)_2](PF_6)_2$ (M = Pt (**5**), Pd (**6**)). The additional zerovalent metal atom is incorporated into the terminal position of the trinuclear aggregation, resulting in a $d^9-d^{10}-d^9$ configuration *via* one electron transfer from the additional metal to the diplatinum core. The three metal atoms are joined by two metal−metal $\sigma$-bonds (average Pt−Pt = 2.724(2) Å (**5**), Pt−Pt/Pd = 2.690(1) Å) and are symmetrically bridged by two dpmp ligands, to form a linearly ordered trinuclear structure (Pt−Pt−M = 178.66(8)° (**5**), 180.0° (**6**)). The similar reactions of the *anti*-dimer (**2**) with $[M_3(RNC)_6]$ led to a formation of the A-frame trinuclear clusters, *A-frame*-$[Pt_2M(\mu\text{-dpmp})_2(RNC)_2](PF_6)_2$ (**7**, M = Pt, R = Xyl; **8**, M = Pd, R = Mes). The three metal atoms are joined by two metal−metal bonds (Pt−M = 2.6039(7) Å (**7**), 2.599(3) Å (**8**)) and asymmetrically bridged by two dpmp ligands, resulting in a so-called trimetallic A-frame structure (Pt−M−Pt = 76.76(3)° (**7**), 78.5(1)° (**8**)). The additional metal is trapped into the middle position of the trinuclear core, through the insertion of $d^{10}$ $ML_2$ fragment into the Pt−Pt $\sigma$-bond, which is interestingly contrasted with the terminal position observed in the reactions of the *syn*-dimer.



## Introduction

Metal−metal-bonded small-size clusters of platinum and palladium have been of potential interest as minimal models for the surface of heterogeneous catalysts and as new homogeneous catalysts and photo- and electrochemical materials. The structures and properties can be modified by varying synthetic strategy and choice of organic ligands. Extensive studies have already been performed on dinuclear Pt(I) and Pd(I) complexes bridged by bis(diphenylphosphino)methane (dppm),[1] with regard to the ability to coordinate small molecules *via* additions across the metal−metal bond. Recently studied platinum and palladium systems have shifted to trinuclear complexes in order to mimic metal surfaces and explore new catalytic behaviors which are not established by a mononuclear center. In designing small-size clusters, one of the most significant problems is how to stabilize the cluster core to resist cluster fragmentation during chemical reactions, and thus, the choice of supporting ligands such as multidentate phosphines is important. The most successful trinuclear system recently studied is the 42-valence electron triplatinum complex $[Pt_3(\mu\text{-dppm})_3(\mu_3\text{-CO})]^{2+}$, which could provide a unsaturated reaction site composed of three metal atoms, various small molecules, and metal fragments being introduced to the coordinatively unsaturated $Pt_3$ triangular face.[2]

We have systematically prepared and characterized metal−metal bonded di-, tri-, and high-nuclear platinum

† Present address: Department of Chemistry, Faculty of Science, Nara Women's University, Nara-shi, Nara 630, Japan.

(1) (a) Puddephatt, R. J. *Chem. Soc. Rev.* **1983**, *12*, 99. (b) Balch, A. P. In *Homogeneous Catalysis with Metal Phosphine Complexes*; Pignolet, L. H., Ed.; Plenum Press: New York, 1983; p 167. (c) Chaudret, B.; Delavaux, B.; Poilblanc, R. *Coord. Chem. Rev.* **1988**, *86*, 191.

S0276-7333(97)00724-3 CCC: $15.00 
Publication on Web 01/01/1998

and palladium complexes supported by bidentate phosphine ligands.[3] By utilization of electrochemical procedures, diplatinum(I) complexes with the bridging dppm ligand, $[Pt_2(\mu\text{-dppm})(RNC)_2]^{2+}$,[3b] and those with chelating diphosphine ligands, $[Pt_2(diphos)_2(RNC)_2]^{2+}$,[3f] were synthesized by one electron reduction of mononuclear platinum(II) complexes, where diphos = $Ph_2P(CH_2)_nPPh_2$ ($n$ = 2−4) and *cis*-1,2-bis(diphenylphosphino)ethene (dppen). Tri- and high-nuclear platinum clusters were obtained in the 1.5−2 electron reduction at more negative potentials, where the structures of clusters varied depending on the diphosphine ligands. The A-frame triplatinum complex $[Pt_3(\mu\text{-dppm})_2(RNC)_2]^{2+}$ was obtained with dppm,[3b] whereas the nonbridged linear trinuclear platinum complexes $[\{Pt(dppe)(RNC)\}_2Pt(RNC)_2]^{2+}$ were formed by using dppe ($n$ = 2).[3f] In the latter case, three Pt atoms are joined by only two metal−metal bonds with their square coordination plane being perpendicular to each other. The similar electrochemical procedures of the complexes with bulkier diphosphines, dppen, dppp ($n$ = 3), and 1,2-bis(di-*tert*-butylphosphino)ethane (dtbpe), led to the uptake of a mercury atom from the electrode to form the linear Pt−Hg−Pt mixed-metal complexes $[\{Pt(diphos)(RNC)\}_2Hg]^{2+}$, where the central metal has no organic ligands.[3g] When those diphosphines that contain a long methylene carbon chain ($n$ = 4−6) were used, the Hg−Pt high-nuclear clusters $[Pt_6Hg(diphos)_2(RNC)_8]$ ($n$ = 4), $[Pt_6Hg_2(diphos)_2(RNC)_8]$ ($n$ = 5, 6), and $[Pt_6Hg_2(diphos)_3(RNC)_6]$ ($n$ = 5, 6) were obtained, with one or two Hg atoms incorporated in between the two $Pt_3$ triangular clusters connected by diphosphines.[3d]

Recently, the tridentate phosphine ligand bis((diphenylphosphino)methyl)phenylphosphine (dpmp) has attracted our attention because the dpmp ligand has versatile bridging and chelating coordination behaviors for di- and trinuclear metal centers.[4−6] The chemistry of linearly-ordered small-size rhodium clusters has systematically been studied by Balch and his co-workers,[4,5] whereas the corresponding chemistry of Pt and Pd has been largely unexplored. We wish to report herein the reaction of $[Pt_2(RNC)_6]^{2+}$ (R = 2,6-xylyl (Xyl) and 2,4,6-mesityl (Mes)) with dpmp, which afforded isomeric diplatinum complexes, *syn*- and *anti*-$[Pt_2(\mu\text{-dpmp})_2(XylNC)_2]^{2+}$ (**1** and **2**), where the central P atoms of dpmp ligands bind to the same metal center in the *syn* form and to the different metal centers in the *anti* form. The *syn*- and *anti*-dimers proved to be good precursors of trimetallic systems and eventually trapped a zerovalent platinum or palladium atom to afford novel linear trinuclear clusters, *linear*-$[Pt_2M(\mu\text{-dpmp})_2(RNC)_2]^{2+}$, and A-frame trinuclear clusters, *A-frame*-$[Pt_2M(\mu\text{-dpmp})_2(RNC)_2]^{2+}$, respectively (M = Pt, Pd). Preliminary results have already been reported.[7,8]

## Experimental Section

Dichloromethane, acetone, and acetonitrile were distilled over calcium hydride and diethyl ether was distilled over lithium aluminum hydride prior to use. Other reagents were of the best commercial grade and were used as received. Complexes $[Pt_2(RNC)_6](PF_6)_2$,[9] $[Pt_3(RNC)_6]$,[10] $[Pd_3(RNC)_6]$[11] (R = 2,6-xylyl (Xyl) and 2,4,6-mesityl (Mes)), and $[Cu(CH_3CN)_4]PF_6$,[12] bis((diphenylphosphino)methyl)phenylphosphine (dpmp),[13] and 2,6-xylyl and 2,4,6-mesityl isocyanides[14] were prepared by the known methods. All reactions were carried out under a nitrogen atmosphere with standard Schlenk and vacuum line techniques.

**Measurements.** $^1H$ NMR spectra were measured on a Bruker AC250 instrument at 250 MHz at room temperature. Chemical shifts were calibrated to tetramethylsilane as an external reference. $^{31}P\{^1H\}$ NMR spectra were recorded by the same instrument at 101 MHz, chemical shifts being calibrated to 85% $H_3PO_4$ as an external reference. Infrared and electronic absorption spectra were recorded with Jasco FT/IR-5300 and Ubest-30 spectrometers, respectively.

**Preparation of *syn*-$[Pt_2(\mu\text{-dpmp})_2(RNC)_2](PF_6)_2$ (1a, R = Xyl; 1b, R = Mes) and *anti*-$[Pt_2(\mu\text{-dpmp})_2(RNC)_2](PF_6)_2$ (2a, R = Xyl; 2b, R = Mes).** To a dichloromethane solution (50 mL) of $[Pt_2(XylNC)_6](PF_6)_2$ (925 mg, 0.630 mmol) was added dpmp (761 mg, 1.502 mmol), and the solution was stirred at room temperature for 12 h. The solution was concentrated under reduced pressure to ca. 20 mL, and diethyl ether (ca. 5 mL) was slowly added to the solution. The resultant solution was allowed to stand at room temperature for ca. 12−24 h to give yellow needles of *syn*-$[Pt_2(\mu\text{-dpmp})_2(XylNC)_2](PF)_2$ (**1a**), which were collected, washed with diethyl ether, and dried in vacuo (yield 57%, 702 mg). The mother liquor was concentrated to dryness, and the residue was crystallized from a $CH_2Cl_2$ (∼15 mL)/$Et_2O$ (2−5 mL) mixed solvent to afford orange

(2) (a) Puddephatt, R. J.; Manojlovic-Muir, L.; Muir, K. W. *Polyhedron* **1990**, *9*, 2767 and references cited therein. (b) Payne, N. C.; Ramachandran, R.; Schoettel, G.; Vittal, J. J.; Puddephatt, R. J. *Inorg. Chem.* **1991**, *30*, 4048. (c) Jennings, M. C.; Schoettel, G.; Roy, S.; Puddephatt, R. J. *Organometallics* **1991**, *10*, 580. (d) Xiao, J.; Vittal, J. J.; Puddephatt, R. J. *J. Am. Chem. Soc.* **1993**, *115*, 7882. (e) Xiao, J.; Puddephatt, R. J. *J. Am. Chem. Soc.* **1994**, *116*, 1129. (f) Xiao, J.; Hao, L.; Puddephatt, R. J. *Organometallics* **1995**, *14*, 2194.

(3) (a) Yamamoto, Y.; Takahashi, K.; Yamazaki, H. *J. Am. Chem. Soc.* **1986**, *108*, 2458. (b) Yamamoto, Y.; Yamazaki, H. *Organometallics* **1993**, *12*, 933. (c) Tanase, T.; Kudo, Y.; Ohno, M.; Kobayashi, K.; Yamamoto, Y. *Nature* **1990**, *344*, 526. (d) Tanase, T.; Horiuchi, T.; Kobayashi, K.; Yamamoto, Y. *J. Organomet. Chem.* **1992**, *440*, 1. (e) Tanase, T.; Kawahara, K.; Ukaji, H.; Kobayashi, K.; Yamazaki, H.; Yamamoto, Y. *Inorg. Chem.* **1993**, *32*, 3682. (f) Tanase, T.; Ukaji, H.; Kudo, Y.; Ohno, M.; Kobayashi, K.; Yamamoto, Y. *Organometallics* **1994**, *13*, 1301. (g) Tanase, T.; Yamamoto, Y. Puddephatt, R. J. *Organometallics*, **1996**, *15*, 1502. (h) Tanase, T.; Nomura, T.; Fukushima, T.; Yamamoto, Y.; Kobayashi, K. *Inorg. Chem.* **1993**, *32*, 4578. (i) Tanase, T.; Fukushima, T.; Nomura, T.; Yamamoto, Y.; Kobayashi, K. *Inorg. Chem.* **1994**, *33*, 32. (j) Yamamoto, Y.; Tanase, T.; Mori, I.; Nakamura, Y. *J. Chem. Soc., Dalton Trans.* **1994**, 3191. (k) Tanase, T.; Ukaji, H.; Yamamoto, Y. *J. Chem. Soc., Dalton Trans.* **1996**, 3059.

(4) Balch, A. L. In *Progress in Inorganic Chemistry*; Lippard, S. J., Ed.; Wiley: New York, 1994; Vol. 41, p 239.

(5) (a) Guimerans, R. R.; Olmstead, M. M.; Balch, A. L. *J. Am. Chem. Soc.* **1983**, *105*, 1677. (b) Olmstead, M. M.; Guimerans, R. R.; Balch, A. L. *Inorg. Chem.* **1983**, *22*, 2473. (c) Olmstead, M. M.; Guimerans, R. R.; Farr, J. P.; Balch, A. L. *Inorg. Chim. Acta* **1983**, *75*, 199. (d) Balch, A. L.; Guimerans, R. R.; Olmstead, M. M. *J. Organomet. Chem.* **1984**, *268*, C38. (e) Balch, A. L.; Fossett, L. A.; Guimerans, R. R.; Olmstead, M. M. *Organometallics* **1985**, *4*, 781. (f) Balch, A. L.; Guimerans, R. R.; Linehan, J. *Inorg. Chem.* **1985**, *24*, 290. (g) Balch, A. L.; Linehan, J. C.; Olmstead, M. M. *Inorg. Chem.* **1986**, *25*, 3937. (h) Balch, A. L.; Fossett, L. A. Olmstead, M. M. *Organometallics* **1987**, *6*, 1827. (i) Balch, A. L.; Fossett, L. A.; Linehan, J. Olmstead, M. M. *Organometallics* **1990**, *5*, 1638. (j) Balch, A. L.; Davis, B. J.; Olmstead, M. M. *Inorg. Chem.* **1990**, *29*, 3066. (k) Balch, A. L.; Catalano, V. J.; Olmstead, M. M. *J. Am. Chem. Soc.* **1990**, *112*, 2010.

(6) Li, P.; Che, C.-M.; Peng, S.-M.; Liu, S.-T.; Zhou, Z.-Y.; Mak, T. C. W. *J. Chem. Soc., Dalton Trans.* **1993**, 189.

(7) Yamamoto, Y.; Tanase, T.; Ukaji, H.; Hasegawa, M.; Igoshi, T.; Yoshimura, K. *J. Organomet. Chem.*, **1995**, *498*, C23.

(8) Tanase, T.; Ukaji, H.; Igoshi, T.; Takahata, H.; Toda, H.; Yamamoto, T. *J. Organomet. Chem.* in press.

(9) (a) Yamamoto, Y.; Takahashi, K.; Yamazaki, H. *Chem. Lett.* **1985**, 201. (b) Yamamoto, Y.; Takahashi, K.; Matsuda, K.; Yamazaki, H. *J. Chem. Soc., Dalton Trans.* **1987**, 1833.

(10) Green, M.; Howard, J. A.; Spencer, J. L.; Stone, F. G. A. *J. Chem. Soc., Chem. Commun.* **1975**, 3.

(11) Christofides, A. *J. Organomet. Chem.* **1983**, *259*, 355.

(12) Kubas, G. J. *Inorg. Synth.* **1979**, *19*, 90.

(13) Appell, R.; Geisler, K.; Scholer, H. F. *Chem. Ber.* **1979**, *112*, 648.

(14) Walborsky, H. M.; Niznik, G. E. *J. Org. Chem.* **1972**, *37*, 187.

blocked-shape crystals of *anti*-$[Pt_2(\mu\text{-dpmp})_2(XylNC)_2](PF_6)_2\cdot 2CH_2Cl_2$ (**2a**·$2CH_2Cl_2$) with a small amount of yellow **1a**. Recrystallizarion of the crude compound **2a**·$2CH_2Cl_2$ from a $CH_2Cl_2/Et_2O$ mixed solvent gave pure orange crystals of **2a**·$2CH_2Cl_2$ in 29% yield (388 mg). Analytical and spectral data for **1a** are as follows. Anal. Calcd for $C_{82}H_{76}N_2Pt_2P_8F_{12}$: C, 50.37; H, 3.92; N, 1.43. Found: C, 49.77; H, 3.96; N, 1.74. IR (Nujol): 2153 (N≡C), 839 ($PF_6$) $cm^{-1}$. UV−vis (in $CH_2Cl_2$): $\lambda_{max}$ (log $\epsilon$) 322 (4.12) nm. $^1H$ NMR (in acetone-$d_6$): $\delta$ 1.45, 1.94 (s, *o*-Me), 3.5−5.8 (m, $CH_2$), 6.8−8.1 (m, Ar). The $^{31}P\{^1H\}$ NMR spectrum in acetone-$d_6$ was broad and featureless. A slow recrystallization of **1a** from a dichloromethane/diethyl ether mixed solvent yielded large blocked-shape crystals of **1a**·$2CH_2Cl_2$ which were suitable for X-ray crystallography. Analytical and spectral data for **2a**·$2CH_2Cl_2$ are as follows. Anal. Calcd for $C_{84}H_{80}N_2Pt_2P_8F_{12}Cl_4$: C, 47.47; H, 3.79; N, 1.32. Found: C, 47.81; H, 3.91; N, 1.46. IR (Nujol): 2164, 2130 (N≡C), 839 ($PF_6$) $cm^{-1}$. UV−vis (in $CH_2Cl_2$): $\lambda_{max}$ (log $\epsilon$) 327 (4.11) nm. $^1H$ NMR (in acetone-$d_6$): $\delta$ 1.71 (s, *o*-Me), 4.2−6.0 (m, $CH_2$), 6.4−8.5 (m, Ar). The $^{31}P\{^1H\}$ NMR spectrum in acetone-$d_6$ was broad and featureless. A slow recrystallization of **2a** from a dichloromethane/diethyl ether mixed solvent yielded large block-shaped crystals of **2a**·$CH_2Cl_2\cdot H_2O$ which were suitable for X-ray crystallography.

Complexes **1b** and **2b** were prepared by the procedure similar to that for **1a** and **2a**. To a dichloromethane solution (50 mL) of $[Pt_2(MesNC)_6](PF_6)_2$ (1050 mg, 0.677 mmol) was added dpmp (761 mg, 1.502 mmol), and the solution was stirred at room temperature for 24 h. The solution was concentrated under reduced pressure to ca. 20 mL, and diethyl ether (ca. 5 mL) was slowly added to the solution. The resultant solution was allowed to stand at room temperature for ca. 12−24 h to give blocked-shape orange crystals of *anti*-$[Pt_2(\mu\text{-dpmp})_2(MesNC)_2](PF)_2\cdot 0.5CH_2Cl_2$ (**2b**·$0.5CH_2Cl_2$), which were collected, washed with diethyl ether, and dried in vacuo (yield 33%, 453 mg). The mother liquor was concentrated to dryness, and the residue was crystallized from a $CH_2Cl_2$ (∼15 mL)/$Et_2O$ (2−5 mL) mixed solvent to afford yellow needles of *syn*-$[Pt_2(\mu\text{-dpmp})_2(MesNC)_2](PF_6)_2\cdot 0.5CH_2Cl_2$ (**2b**·$0.5CH_2Cl_2$) in 18% yield (247 mg). Analytical and spectral data for **1b**·$0.5CH_2Cl_2$ are as follows. Anal. Calcd for $C_{84.5}H_{81}N_2Pt_2P_8F_{12}Cl$: C, 50.10; H, 4.03; N, 1.38. Found: C, 49.85; H, 4.00; N, 1.52. IR (Nujol): 2155 (N≡C), 840 ($PF_6$) $cm^{-1}$. UV−vis (in $CH_2Cl_2$): $\lambda_{max}$ (log $\epsilon$) 322 (4.14) nm. $^1H$ NMR (in acetone-$d_6$): $\delta$ 1.40, 1.89 (s, *o*-Me), 2.17, 2.24 (s, *p*-Me), 3.4−5.7 (m, $CH_2$), 6.6−8.1 (m, Ar). The $^{31}P\{^1H\}$ NMR spectrum in acetone-$d_6$ was broad and featureless. Analytical and spectral data for **2b**·$0.5CH_2Cl_2$ are as follows. Anal. Calcd for $C_{84.5}H_{81}N_2Pt_2P_8F_{12}Cl$: C, 50.10; H, 4.03; N, 1.38. Found: C, 50.02; H, 4.02; N, 1.53. IR (Nujol): 2172, 2141 (N≡C), 839 ($PF_6$) $cm^{-1}$. UV−vis (in $CH_2Cl_2$): $\lambda_{max}$ (log $\epsilon$) 327 (4.07) nm. $^1H$ NMR (in acetone-$d_6$): $\delta$ 1.66 (s, *o*-Me), 2.19 (s, *p*-Me), 4.2−6.0 (m, $CH_2$), 6.4−8.5 (m, Ar). The $^{31}P\{^1H\}$ NMR spectrum in acetone-$d_6$ was broad and featureless.

**Preparation of *syn*-$[Pt_2(\mu\text{-dpmp})_2(XylNC)](PF_6)_2$ (3).** Compounds **1a** (50.1 mg, 0.0256 mmol) and $[Cu(CH_3CN)_4](PF_6)$ (10.2 mg, 0.0274 mmol) were dissolved in dichloromethane (10 mL), and the solution was stirred at room temperature for 2 h. The solvent was removed under reduced pressure, and the residue was crystallized from an acetone/diethyl ether mixed solvent to afford blocked-shape yellow crystals of *syn*-$[Pt_2(\mu\text{-dpmp})_2(XylNC)](PF_6)_2$ (**3**) in 71% yield (33.2 mg). Anal. Calcd for $C_{73}H_{67}NPt_2P_8F_{12}$: C, 48.06; H, 3.70; N, 0.77. Found: C, 47.66; H, 3.63; N, 0.94. IR (Nujol): 2118 (N≡C), 833 ($PF_6$) $cm^{-1}$. UV−vis (in $CH_2Cl_2$): $\lambda_{max}$ (log $\epsilon$) 322 (4.12), 418 $(3.21)^{sh}$ nm. $^1H$ NMR (in acetone-$d_6$): $\delta$ 1.76 (s, *o*-Me), 4.2−6.2 (m, $CH_2$), 6.7−8.4 (m, Ar). The $^{31}P\{^1H\}$ NMR spectrum in acetone-$d_6$ showed complicated spectral patterns in the range of −70 to 10 ppm. Recrystallization of **3** from a dichloromethane/diethyl ether mixed solvent gave blocked-shape crystals of **2a**·$2CH_2Cl_2$ which were suitable for X-ray crystallography.

**Preparation of *anti*-$[Pt_2(\mu\text{-dpmp})_2(XylNC)](PF_6)_2$ (4).** Complex **1a** (107 mg, 0.0547 mmol) was dissolved in 40 mL of acetonitrile, and the solution was heated at reflux for 24 h. The solution was concentrated under reduced pressure to dryness, and the residue was crystallized from a dichloromethane/diethyl ether mixed solvent to give orange-yellow blocked-shape crystals of *anti*-$[Pt_2(\mu\text{-dpmp})_2(XylNC)](PF_6)_2$ (**4**) in 56% yield (56 mg). The starting complex **1a** and its isomer **2a** were obtained in 30% and 3% yields, respectively, from the mother liquor. Complex **4** was also obtained from **2a** by the similar method. Anal. Calcd for $C_{73}H_{67}NPt_2P_8F_{12}$: C, 48.06; H, 3.70; N, 0.77. Found: C, 47.95; H, 3.84; N, 0.94. IR (Nujol): 2160 (N≡C), 835 ($PF_6$) $cm^{-1}$. UV−vis (in $CH_2Cl_2$): $\lambda_{max}$ (log $\epsilon$) 329 (4.01), 373 $(3.73)^{sh}$, 431 $(2.91)^{sh}$ nm. $^1H$ NMR (in acetone-$d_6$): $\delta$ 1.70 (s, *o*-Me), 4.2−6.1 (m, $CH_2$), 6.4−8.6 (m, Ar). The $^{31}P\{^1H\}$ NMR spectrum in acetone-$d_6$ showed complicated spectral patterns in the range of −85 to 25 ppm.

**Preparation of *linear*-$[Pt_2M(\mu\text{-dpmp})_2(XylNC)_2](PF_6)_2$ (5, M = Pt; 6, M = Pd).** Complex $[Pt_3(XylNC)_6]$ (543 mg, 0.394 mmol) was added to a dichloromethane solution (50 mL) containing *syn*-$[Pt_2(\mu\text{-dpmp})_2(XylNC)_2](PF_6)_2$ (**1a**) (768 mg, 0.393 mmol). The resultant solution was stirred at room temperature for 12 h. The solvent was removed under reduced pressure, and the residue was crystallized from an acetone/diethyl ether mixed solvent to afford reddish orange crystals of *linear*-$[Pt_3(\mu\text{-dpmp})_2(XylNC)_2](PF_6)_2\cdot(CH_3)_2CO$ (**5**·$(CH_3)_2CO$) in 88% yield (761 mg) based on **1a**. Anal. Calcd for $C_{85}H_{82}N_2Pt_3P_8F_{12}O$: C, 46.23; H, 3.74; N, 1.27. Found: C, 45.87; H, 4.01; N, 1.26. IR (Nujol): 2130 (N≡C), 841 ($PF_6$) $cm^{-1}$. UV−vis (in $CH_2Cl_2$): $\lambda_{max}$ (log $\epsilon$) 297 (3.92), 360 (4.02), 389 (4.13) nm. $^1H$ NMR (in $CDCl_3$): $\delta$ 1.40 (s, *o*-Me), 4.5−5.3 (m, $CH_2$), 6.6−8.2 (m, Ar). $^{13}C$ NMR (in $CDCl_3$): $\delta$ 17.8 (s, *o*-Me). $^{31}P\{^1H\}$ NMR (in $CDCl_3$): $\delta$ −16.8 (m, 2P, $^1J_{PtP}$ = 2777 Hz, $^2J_{PtP}$ = 84 Hz), 1.1 (m, 1P, $^1J_{PtP}$ = 2946 Hz, $^2J_{PtP}$ = 84 Hz). Recrystallization of **5**·$(CH_3)_2CO$ from a dichloromethane/diethyl ether mixed solvent gave prismatic crystals of **5**·$CH_2Cl_2$ which were suitable for X-ray crystallography. The similar procedure by using $[Pd_3(XylNC)_6]$ yielded *linear*-$[Pt_2Pd(\mu\text{-dpmp})_2(XylNC)_2](PF_6)_2\cdot(CH_3)_2CO$ (**6**·$(CH_3)_2CO$) in 63% yield base on **1a**. Anal. Calcd for $C_{85}H_{82}N_2Pt_2PdP_8F_{12}O$: C, 48.16; H, 3.90; N, 1.32. Found: C, 48.07; H, 4.22; N, 1.32. IR (Nujol): 2133 (N≡C), 841 ($PF_6$) $cm^{-1}$. UV−vis (in $CH_2Cl_2$): $\lambda_{max}$ (log $\epsilon$) 351 (3.76), 393 (3.89), 435 (3.98) nm. $^1H$ NMR (in $CDCl_3$): $\delta$ 1.37, 1.49 (s, *o*-Me), 4.2−5.4 (m, $CH_2$), 6.6−8.2 (m, Ar). $^{13}C$ NMR (in $CDCl_3$): $\delta$ 17.8, 17.9 (s, *o*-Me). $^{31}P\{^1H\}$ NMR (in $CDCl_3$): $\delta$ −16.1 (m, 1P, $^1J_{PtP}$ = 2774 Hz, $^2J_{PtP}$ = 81 Hz), 1.1 (m, 1P, $^1J_{PtP}$ = 2802 Hz, $^2J_{PtP}$ = 88 Hz), 2.4 (m, 1P). A slow recrystallization of **6**·$(CH_3)_2CO$ from an acetone/diethyl ether mixed solvent gave large prismatic crystals of **6**·$4(CH_3)_2CO$ which were suitable for X-ray crystallography.

**Preparation of *A-frame*-$[Pt_2M(\mu\text{-dpmp})_2(RNC)_2](PF_6)_2$ (7, M = Pt, R = Xyl; 8, M = Pd, R = Mes).** To a dichloromethane solution containing *anti*-$[Pt_2(\mu\text{-dpmp})_2(XylNC)_2](PF_6)_2\cdot 2CH_2Cl_2$ (**2a**·$2CH_2Cl_2$) (266 mg, 0.125 mmol) was added $[Pt_3(XylNC)_6]$ (159 mg, 0.116 mmol). The resultant solution was stirred at room temperature for 12 h. The solvent was removed under reduced pressure, and the residue was crystallized from a dichloromethane/diethyl ether mixed solvent to give yellow crystals of *A-frame*-$[Pt_3(\mu\text{-dpmp})_2(XylNC)_2](PF_6)_2$ (**7**) in 70% yield (188 mg) based on **2a**. Anal. Calcd for $C_{82}H_{76}N_2Pt_3P_8F_{12}$: C, 45.80; H, 3.56; N, 1.30. Found: C, 45.71; H, 3.50; N, 1.23. IR (Nujol): 2130 (N≡C), 839 ($PF_6$) $cm^{-1}$. UV−vis (in $CH_2Cl_2$): $\lambda_{max}$ (log $\epsilon$) 311 (3.99) nm. $^1H$ NMR (in acetone-$d_6$): $\delta$ 1.76 (s, *o*-Me), 4.6−5.8 (m, $CH_2$), 6.9−8.4 (m, Ar). $^{31}P\{^1H\}$ NMR (in $CDCl_3$): $\delta$ −34.0 (m, 1P, $^1J_{PtP}$ = 2863 Hz, $^2J_{PP}$ = 412 Hz), 1.9 (m, 1P, $^1J_{PtP}$ = 2581 Hz, $^2J_{PtP}$ = 240 Hz), 23.0 (m, 1P, $^1J_{PtP}$ = 2900 Hz, $^2J_{PP}$ = 412 Hz). The similar procedure by using *anti*-$[Pt_2(\mu\text{-dpmp})_2(MesNC)_2](PF_6)_2\cdot 0.5CH_2Cl_2$ (**2b**) and $[Pd_3(MesNC)_6]$ as starting materials afforded *A-frame*-$[Pt_2Pd(\mu\text{-dpmp})_2(MesNC)_2](PF_6)_2$ (**8**) in 31% yield base on **2b**. Anal. Calcd for $C_{84}H_{80}N_2F_{12}P_8Pt_2Pd$: C, 48.28; H, 3.86;

**Table 1. Crystallographic and Experimental Data for 1a·2$CH_2Cl_2$, 2a·1.5$CH_2Cl_2$·$H_2O$, 3·2$CH_2Cl_2$, and 4**

| compd | **1a**·2$CH_2Cl_2$ | **2a**·1.5$CH_2Cl_2$·$H_2O$ | **3**·2$CH_2Cl_2$ | **4** |
|---|---|---|---|---|
| formula | $C_{84}H_{80}N_2P_8F_{12}Pt_2Cl_4$ | $C_{83.5}H_{81}N_2P_8F_{12}Pt_2Cl_3O$ | $C_{75}H_{71}NP_8F_{12}Pt_2Cl_4$ | $C_{73}H_{67}NP_8F_{12}Pt_2$ |
| M | 2125.33 | 2100.88 | 1994.16 | 1824.29 |
| cryst syst | orthorhombic | triclinic | monoclinic | triclinic |
| space group | *Pbca* (No. 61) | $P\bar{1}$ (No. 2) | *C*2/*c* (No. 15) | $P\bar{1}$ (No. 2) |
| *a*/Å | 43.077(9) | 13.528(8) | 46.23(1) | 16.490(2) |
| *b*/Å | 22.749(8) | 29.89(2) | 12.667(4) | 16.615(2) |
| *c*/Å | 17.333(5) | 12.250(6) | 26.728(8) | 13.553(1) |
| α/deg | | 98.32(6) | | 90.530(8) |
| *β*/deg | | 99.41(5) | 104.70(6) | 101.427(7) |
| *γ*/deg | | 103.06(5) | | 90.968(9) |
| *V*/Å$^3$ | 16 985 | 4675 | 15139 | 3639 |
| Z | 8 | 2 | 8 | 2 |
| *T*/°C | −96 | 23 | −147 | 23 |
| $D_{calcd}$/g cm$^{-1}$ | 1.662 | 1.492 | 1.750 | 1.665 |
| *μ*/cm$^{-1}$ | 36.26 | 33.05 | 40.61 | 41.24 |
| scan method | *ω* | *ω*−2*θ* | *ω* | *ω*−2*θ* |
| 2$\theta_{max}$/deg | 47 | 50 | 50 | 50 |
| *h*,*k*,*l* range | +*h*,+*k*,+*l* | +*h*,±*k*,±*l* | +*h*,+*k*,±*l* | +*h*,±*k*,±*l* |
| no. of data | 13586 | 16 550 | 10 553 | 12 810 |
| no. of obsd data | 6927 ($I > 3\sigma(I)$) | 10 536 ($I > 3\sigma(I)$) | 6111 ($I > 3\sigma(I)$) | 7021 ($I > 3\sigma(I)$) |
| solution | direct methods (SIR92) | Patterson method | direct methods (SIR92) | Patterson method |
| no. of params | 620 | 987 | 570 | 865 |
| data/param | 11.17 | 10.67 | 10.72 | 8.12 |
| $R^a$ | 0.052 | 0.051 | 0.049 | 0.044 |
| $R_w{}^a$ | 0.051 | 0.064 | 0.048 | 0.045 |
| GOF$^b$ | 1.43 | 1.97 | 1.30 | 1.30 |
| $\rho_{max}$, e Å$^{-3}$ | 0.98 | 2.11 | 1.25 | 1.32 |

$^a$ $R = \Sigma||F_o| - |F_c||/\Sigma|F_o|$; $R_w = [\Sigma w(|F_o| - |F_c|)^2/\Sigma w|F_o|^2]^{1/2}$ ($w = 1/\sigma^2(F_o)$). $^b$ GOF = $[\Sigma w(|F_o| - |F_c|)^2/(N_o - N_p)]^{1/2}$ ($N_o$ = no. of data, $N_p$ = no. of variables).

**Table 2. Crystallographic and Experimental Data for 5·$CH_2Cl_2$, 6·4$(CH_3)_2CO$, 7, and 8**

| compd | **5**·$CH_2Cl_2$ | **6**·4$(CH_3)_2CO$ | **7** | **8** |
|---|---|---|---|---|
| formula | $C_{83}H_{78}N_2P_8F_{12}Pt_3Cl_2$ | $C_{94}H_{100}N_2P_8F_{12}Pt_2PdCl_3O_4$ | $C_{82}H_{76}N_2P_8F_{12}Pt_3$ | $C_{84}H_{80}N_2P_8F_{12}Pt_2Pd$ |
| $M_r$ | 2235.49 | 2294.19 | 2150.56 | 2089.92 |
| cryst syst | monoclinic | triclinic | monoclinic | monoclinic |
| space group | $P2_1/n$ (No. 14) | $P\bar{1}$ (No. 2) | *C*2/*c* (No. 15) | *C*2/*c* (No. 15) |
| *a*/Å | 22.865(7) | 13.906(7) | 15.353(2) | 22.209(6) |
| *b*/Å | 22.626(6) | 16.084(7) | 23.436(3) | 23.777(4) |
| *c*/Å | 16.827(4) | 11.866(7) | 22.974(8) | 20.136(3) |
| α/deg | | 95.68(4) | | |
| *β*/deg | 90.19(3) | 110.09(4) | 102.96(2) | 117.44(3) |
| *γ*/deg | | 76.68(4) | | |
| *V*/Å$^3$ | 8705 | 2425 | 8056 | 9436 |
| Z | 4 | 1 | 4 | 4 |
| *T*/°C | −100 | 23 | 23 | -147 |
| $D_{calcd}$/g cm$^{-1}$ | 1.706 | 1.571 | 1.773 | 1.471 |
| *μ*/cm$^{-1}$ | 50.67 | 32.88 | 54.78 | 33.33 |
| scan method | *ω*−2*θ* | *ω*−2*θ* | *ω*−2*θ* | *ω*−2*θ* |
| 2*θ* max/° | 45 | 50 | 50 | 45 |
| *h*,*k*,*l* range | +*h*, +*k*, ±*l* | +*h*, ±*k*, ±*l* | +*h*, +*k*, ±*l* | +*h*, +*k*, ±*l* |
| no. of data | 12 057 | 7748 | 7032 | 6343 |
| no. of obsd data | 5485 ($I > 3\sigma(I)$) | 4251($I > 3\sigma(I)$) | 4326 ($I > 3\sigma(I)$) | 2783 ($I > 3\sigma(I)$) |
| solution | direct methods (SAPI90) | direct methods (MITHRIL) | direct methods (MITHRIL) | Patterson method |
| no. of params | 567 | 517 | 483 | 259 |
| data/param | 9.67 | 8.22 | 8.96 | 10.75 |
| $R^a$ | 0.079 | 0.036 | 0.035 | 0.085 |
| $R_w{}^a$ | 0.084 | 0.033 | 0.041 | 0.086 |
| GOF$^b$ | 2.49 | 1.68 | 1.30 | 2.46 |
| $\rho_{max}$, e Å$^{-3}$ | 3.37 | 1.12 | 1.01 | 1.90 |

$^a$ $R = \Sigma||F_o| - |F_c||/\Sigma|F_o|$; $R_w = [\Sigma w(|F_o| - |F_c|)^2/\Sigma w|F_o|^2]^{1/2}$ ($w = 1/\sigma^2(F_o)$). $^b$ GOF = $[\Sigma w(|F_o| - |F_c|)^2/(N_o - N_p)]^{1/2}$ ($N_o$ = no. of data, $N_p$ = no. of variables).

N, 1.34. Found: C, 48.33; H, 3.39; N, 1.29. IR (Nujol): 2128 (N≡C), 837 ($PF_6$) cm$^{-1}$. UV−vis ($CH_2Cl_2$): $\lambda_{max}$ (log $\epsilon$) 396 (3.64) nm. $^1$H NMR (acetone-$d_6$): $\delta$ 1.83 (s, *o*-Me), 2.21 (s, *p*-Me), 4.81, 5.12, 5.68 (m, $CH_2$), 6.9−8.2 (m, Ar). $^{31}$P{$^1$H} NMR (acetone-$d_6$): $\delta$ −29.8 (m, $^1J_{PtP}$ = 2805 Hz, $^2J_{PP'}$ = 426 Hz, 1P), −10.2 (m, $^2J_{PtP}$ = 341 Hz, 1P), 16.2 (m, $^1J_{PtP}$ = 2746 Hz, $^2J_{PP'}$ = 426 Hz, 1P).

**X-ray Crystallographic Analyses of 1a·2$CH_2Cl_2$, 2a·1.5$CH_2Cl_2$·$H_2O$, 3·2$CH_2Cl_2$, 4, 5·$CH_2Cl_2$, 6·4$(CH_3)_2CO$, 7, and 8.** Crystal data and experimental conditions are summarized in Tables 1 and 2. All data were collected on a Rigaku AFC5S diffractometer equipped with graphite-monochromated Mo Kα ($\lambda$ = 0.710 69 Å) radiation. Reflection data were corrected for Lorentz−polarization, and absorption effects, by the *ψ*-scan method. The structures of **1a**·2$CH_2Cl_2$ and **3**·2$CH_2Cl_2$ were solved by direct methods with SIR92,[15] that of **5**·$CH_2Cl_2$ was solved with SAPI90,[16] and those of **6**·4$(CH_3)_2CO$ and **7** were solved with MITHRIL.[17] In the structure of **6**, the terminal metal position was refined as a disordered model with Pt and Pd atoms each having 0.5 occupancy. The structures

(15) Burla, M. C.; Camalli, M.; Cascarano, G.; Giacovazzo, C.; Polidori, G.; Spagna, R.; Viterbo, D. *J. Appl. Crystallogr.* **1989**, *22*, 389.
(16) Fan, H.-F. R-SAPI88, Rigaku Corp. Tokyo, Japan, 1988.
(17) Gilmore, G. J. *J. Appl. Crystallogr.* **1984**, *17*, 42

of **2a**·1.5$CH_2Cl_2$·$H_2O$, **4**, and **8** were solved by the Patterson method and were expanded by DIRDIF.[18] In the structure of **8**, the $PF_6$ anion is disordered and refined with two P atoms each having 0.5 occupancy and nine F atoms each having 0.667 multiplicity. The experimental details are supplied as Supporting Information.

Atomic scattering factors and values of $f'$ and $f''$ for Pt, Pd, Cl, P, F, N, and C were taken from the literature.[19] All calculations were carried out on a Digital VAX Station 3100 and a Silicon Graphics Indy Station with the TEXSAN Program System.[20] The perspective views were drawn by using the programs ORTEP-II.[21] A compilation of final atomic parameters for all non-hydrogen atoms is supplied as Supporting Information.

**Molecular Orbital Calculations.** Extended Hückel molecular orbital calculations were carried out by using parameters of the Coulomb integrals and the orbital exponents taken from ref 22 on a IBM PC P-120 computer. For the Pt and Pd d functions, double-$\xi$ expansions were used. The fragment analyses were performed by using program CACAO.[23] Geometrical assumptions were derived from simplifications of the crystal structures. Pt−Pt (or Pd) = 2.70 Å (for models **I** and **II**), 2.60 Å (for models **III** and **IV**), Pt−P = 2.30 Å, P−H = 1.30 Å, Pt−C = 1.95 Å, C−N = 1.15 Å, and N−H = 1.05 Å.

## Results and Discussion

**Preparation and Structures of *syn*- and *anti*-$[Pt_2(\mu\text{-dpmp})_2(RNC)_2](PF_6)_2$ (1 and 2).** Reaction of $[Pt_2(XylNC)_6](PF_6)_2$ with 2 equiv of dpmp in dichloromethane at room temperature afforded a mixture of isomeric diplatinum complexes, **1a** and **2a**, formulated as $[Pt_2(\mu\text{-dpmp})_2(XylNC)_2](PF_6)_2$. The two isomeric complexes **1a** and **2a** could be separated by cycles of recrystallization and were isolated as pure crystalline forms in 57% and 29% yields, respectively. The analogous complexes **1b** and **2b** formulated as $[Pt_2(\mu\text{-dpmp})_2(MesNC)_2](PF_6)_2$ were also obtained from the reaction of $[Pt_2(MesNC)_6](PF_6)_2$ with dpmp in isolated yields of 18% and 33%, respectively. We hereafter refer to **1** and **2** respectively as *syn*- and *anti*-forms on the basis of arrangement of two tridentate phosphine ligands (*vide infra*). The IR spectra of **1** and **2** indicated the presence of terminal isocyanide ligands. Two N≡C stretching bands were observed around 2130−2141 and 2164−2172 $cm^{-1}$ for **2**, whereas one N≡C absorption with a slight shoulder feature at higher energy side was observed around 2153−2155 $cm^{-1}$ for **1**. The $^1H$ NMR spectra of the *syn*-dimers (**1a**,**b**) showed two nonequivalent isocyanide ligands on the basis of *o*-methyl signals at $\delta$ 1.40−1.45 and 1.89−1.94 in a ratio of 1:1, and those of the *anti*-dimers (**2a**,**b**) showed only one kind of isocyanide at $\delta$ 1.66−1.71. The $^{31}P\{^1H\}$ NMR spectra of **1** and **2** at room temperature were very broad and featureless, which were invariant from −80 to 50 °C.

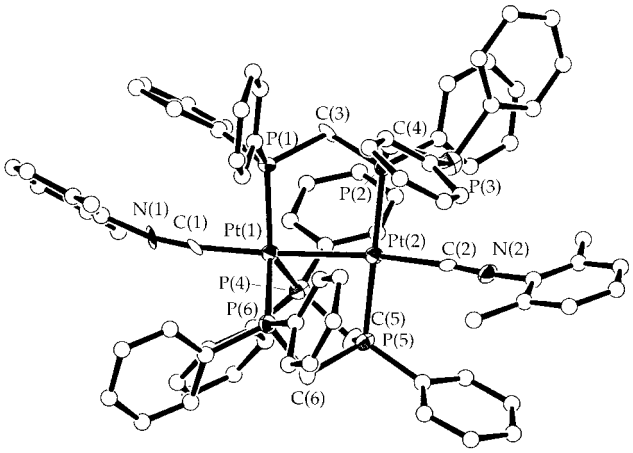


**Figure 1.** ORTEP plot of the complex cation of **1a**, *syn*-$[Pt_2(\mu\text{-dpmp})_2(XylNC)_2](PF_6)_2$. Thermal ellipsoids are drawn at the 30% probability level. The phenyl and xylyl carbon atoms are represented by arbitrary circles, and hydrogen atoms are omitted for clarity.

**Table 3. Selected Bond Lengths (Å) and Angles (deg) for *syn*-$[Pt_2(\mu\text{-dpmp})_2(XylNC)_2](PF_6)_2$ (1a)[a]**

| | | | |
|---|---|---|---|
| Bond Lengths | | | |
| Pt(1)−Pt(2) | 2.7094(8) | Pt(1)−P(1) | 2.331(4) |
| Pt(1)−P(4) | 2.344(4) | Pt(1)−P(6) | 2.360(4) |
| Pt(1)−C(1) | 1.98(1) | Pt(2)−P(2) | 2.316(4) |
| Pt(2)−P(5) | 2.305(4) | Pt(2)−C(2) | 1.97(1) |
| N(1)−C(1) | 1.16(2) | N(1)−C(11) | 1.44(2) |
| N(2)−C(2) | 1.14(2) | N(2)−C(21) | 1.45(2) |
| Bond Angles | | | |
| Pt(2)−Pt(1)−P(1) | 91.53(9) | Pt(2)−Pt(1)−P(4) | 81.48(9) |
| Pt(2)−Pt(1)−P(6) | 83.30(9) | Pt(2)−Pt(1)−C(1) | 176.5(4) |
| P(1)−Pt(1)−P(4) | 122.8(1) | P(1)−Pt(1)−P(6) | 132.3(1) |
| P(1)−Pt(1)−C(1) | 85.0(4) | P(4)−Pt(1)−P(6) | 103.3(1) |
| P(4)−Pt(1)−C(1) | 100.3(4) | P(6)−Pt(1)−C(1) | 99.2(4) |
| Pt(1)−Pt(2)−P(2) | 94.76(9) | Pt(1)−Pt(2)−P(5) | 83.15(9) |
| Pt(1)−Pt(2)−C(2) | 171.8(4) | P(2)−Pt(2)−P(5) | 170.5(1) |
| P(2)−Pt(2)−C(2) | 91.2(4) | P(5)−Pt(2)−C(2) | 91.9(4) |
| Pt(1)−P(1)−C(3) | 112.1(4) | Pt(2)−P(2)−C(3) | 112.6(4) |
| Pt(2)−P(2)−C(4) | 113.1(5) | C(3)−P(2)−C(4) | 106.5(6) |
| Pt(1)−P(4)−C(5) | 112.5(4) | Pt(2)−P(5)−C(5) | 101.9(5) |
| Pt(2)−P(5)−C(6) | 117.0(5) | C(5)−P(5)−C(6) | 102.7(6) |
| Pt(1)−P(6)−C(6) | 105.7(4) | C(1)−N(1)−C(11) | 168(1) |
| C(2)−N(2)−C(21) | 168(1) | Pt(1)−C(1)−N(1) | 172(1) |
| Pt(2)−C(2)−N(2) | 172(1) | | |

[a] Estimated standard deviations are given in parentheses.

The electronic absorption spectra exhibited only slight difference between *syn*- and *anti*-dimers; the $\sigma-\sigma^*$ transition bands appeared at 322 nm for **1** and 327 nm for **2**, significantly red-shifted in comparison with that of $[Pt_2(\mu\text{-dppm})_2(XylNC)_2](PF_6)_2$ (292 nm) (**9**).[3b] The energy difference suggested that the Pt−Pt bonds in **1** and **2** are weaker that of **9**.

The ratio of **1a** and **2a** existing in the reaction mixture varied depending on the solvent used in the reaction. The ratio of **2a** (*anti*-dimer) involved in the reaction mixture increased by using nonpolar solvent, benzene, and that of **1a** (*syn*-dimer) increased with polar solvents such as methanol and acetonitrile.

The structures of the **1a** and **2a** were determined by X-ray crystallography. A perspective view for the complex cation of **1a** is illustrated in Figure 1, and selected bond lengths and angles are listed in Table 3. The complex cation of **1a** consists of an asymmetrical diplatinum(I) center bridge by two dpmp ligands and terminally coordinated by two isocyanide molecules. The

(18) Parthasarathi, V.; Beurskens, P. T.; Slot, H. J. B. *Acta Crystallogr.* **1983**, *A39*, 860.
(19) (a) Cromer, D. T.; Waber, J. T. *International Tables for X-ray Crystallography*; Kynoch Press: Birmingham, England, 1974; Vol. IV. (b) Cromer, D. T. *Acta Crystallogr.* **1965**, *18*, 17.
(20) *TEXSAN Structure Analysis Package*; Molecular Structure Corp.: The Woodlands, TX, 1985.
(21) Johnson, C. K. ORTEP-II, Oak Ridge National Laboratory, Oak Ridge, TN, 1976.
(22) (a) Hoffmann, R. *J. Chem. Phys.* **1963**, *39*, 1397. (b) Hoffmann, R.; Lipscomb, W. N. *J. Chem. Phys.* **1962**, *36*, 2179. (c) Hoffmann, R.; Lipscomb, W. N. *J. Chem. Phys.* **1962**, *36*, 3489. (d) Ammeter, J. H.; Burgi, H.-B.; Thibeault, J. C.; Hoffmann, R. *J. Am. Chem. Soc.* **1978**, *100*, 3686.
(23) Mealli, C.; Prosterpio, D. *J. Chem. Educ.* **1990**, 67, 399.

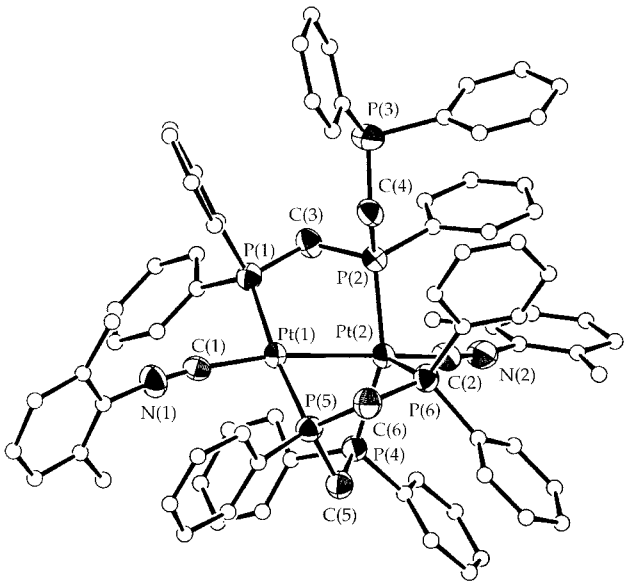


**Figure 2.** ORTEP plot of the complex cation of **2a**, *anti*-$[Pt_2(\mu\text{-dpmp})_2(XylNC)_2](PF_6)_2$. Thermal ellipsoids are drawn at the 40% probability level. The phenyl and xylyl carbon atoms are represented by arbitrary circles, and hydrogen atoms are omitted for clarity.

**Scheme 1**

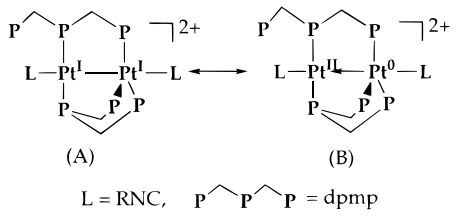


Pt(1)−Pt(2) distance is 2.7094(8) Å, which is fairly long in comparison with typical Pt(I)−Pt(I) $\sigma$-bond lengths. From the geometrical assumption, it is tentatively resulted from a contribution of the Pt(II)←Pt(0) dative bonded structure depicted as B which is mixed into the main Pt(I)−Pt(I) $\sigma$-bonded structure (A) (Scheme 1). The Pt(1) atom is ligated by three phosphorus atoms of dpmp, a terminal carbon atom of XylNC, and the neighboring platinum atom, resulting in a trigonal bipyramidal geometry. Pt(2) and C(1) occupy the apical sites, and the P(1), P(4), and P(6) atoms are involved in the equatorial plane with Pt−P bond lengths of 2.305−2.331 Å. The Pt(2) atom has a square planar geometry coordinated by two phosphorus atoms of dpmp, a terminal carbon atom of XylNC, and the adjacent Pt atom. The dpmp ligands exhibited two different bridging modes. One joins the two metal atoms through a terminal P atom (P(1)) and the inner P atom (P(2)); the remaining terminal P atom (P(3)) is away from the coordination sphere of Pt(2). The other dpmp doubly bridges the two Pt atoms forming a cradle-type structure. The similar double bridging structure was already observed in $[Re_2Cl_3(\mu\text{-dpmp})_2]^+$.[24] Since the central P atoms (P(2) and P(5)) of two dpmp ligands bind to the same metal center (Pt(2)) in **1a**, we denote this arrangement as the *syn*-form. An ORTEP plot of the complex cation of **2a** is given in Figure 2, and selected bond lengths and angles are listed in Table 4. The complex

(24) Cotton, F. A.; Matusz, M. *Inorg. Chem.* **1987**, *26*, 984.

**Table 4. Selected Bond Lengths (Å) and Angles (deg) of *anti*-$[Pt_2(\mu\text{-dpmp})_2(XylNC)](PF_6)_2$ (2a)[a]**

| Bond Lengths | | | |
|---|---|---|---|
| Pt(1)−Pt(2) | 2.683(2) | Pt(1)−P(1) | 2.308(3) |
| Pt(1)−P(5) | 2.278(3) | Pt(1)−C(1) | 1.96(1) |
| Pt(2)−P(2) | 2.289(3) | Pt(2)−P(4) | 2.304(4) |
| Pt(2)−P(6) | 2.470(3) | Pt(2)−C(2) | 1.95(1) |
| N(1)−C(1) | 1.13(1) | N(1)−C(11) | 1.41(2) |
| N(2)−C(2) | 1.17(1) | N(2)−C(21) | 1.42(2) |
| **Bond Angles** | | | |
| Pt(2)−Pt(1)−P(1) | 93.4(1) | Pt(2)−Pt(1)−P(5) | 82.3(1) |
| Pt(2)−Pt(1)−C(1) | 170.7(3) | P(1)−Pt(1)−P(5) | 174.3(1) |
| P(1)−Pt(1)−C(1) | 94.0(3) | P(5)−Pt(1)−C(1) | 90.7(3) |
| Pt(1)−Pt(2)−P(2) | 86.8(1) | Pt(1)−Pt(2)−P(4) | 78.2(1) |
| Pt(1)−Pt(2)−P(6) | 93.85(9) | Pt(1)−Pt(2)−C(2) | 158.9(4) |
| P(2)−Pt(2)−P(4) | 152.2(1) | P(2)−Pt(2)−P(6) | 109.3(1) |
| P(2)−Pt(2)−C(2) | 91.2(4) | P(4)−Pt(2)−P(6) | 95.1(1) |
| P(4)−Pt(2)−C(2) | 94.5(4) | P(6)−Pt(2)−C(2) | 106.6(4) |
| Pt(1)−P(1)−C(3) | 113.3(4) | Pt(2)−P(2)−C(3) | 109.0(4) |
| Pt(2)−P(2)−C(4) | 120.5(4) | C(3)−P(2)−C(4) | 104.4(6) |
| Pt(2)−P(4)−C(5) | 109.1(4) | Pt(1)−P(5)−C(5) | 109.5(4) |
| Pt(1)−P(5)−C(6) | 109.7(4) | C(5)−P(5)−C(6) | 106.8(5) |
| Pt(2)−P(6)−C(6) | 106.4(4) | C(1)−N(1)−C(11) | 172(1) |
| C(2)−N(2)−C(21) | 169(1) | Pt(1)−C(1)−N(1) | 173(1) |
| Pt(2)−C(2)−N(2) | 175(1) | | |

[a] Estimated standard deviations are given in parentheses.

cation is composed of an asymmetrical diplatinum(I) center bridged by two dpmp ligands and terminally coordinated by two isocyanide molecules. The Pt−Pt bond length of 2.683(2) Å is slightly shorter than that of **1a**. The structure of **2a** is essentially similar to **1a** except the geometry around the five-coordinate Pt atom (Pt(2)) and the arrangement of two dpmp ligands. The geometry around the Pt(2) atom is best described as a distorted square pyramidal structure with the Pt(1), P(2), P(4), and C(2) atoms composing a basal plane and the P(6) atom sitting in the apical site. The Pt(2)−P(6) bond length of 2.470(3) Å is significantly longer than those of other P atoms (2.289−2.304 Å). The significant distortion around the Pt(2) atom is seemingly ascribable to the steric bulkiness of the uncoordinated phosphine pendant arm ($Ph_2PCH_2$) connecting to the P(2) atom. The central P atoms of two dpmp ligands bind to different Pt centers, which can be denoted as *anti*-form. Cotton et al. have predicted the presence of *syn*- and *anti*-isomers in the direnium complex $[Re_2Cl_3(\mu\text{-dpmp})_2]^+$, although only the *anti*-form has been isolated and characterized.[24] Now, we have succeeded in isolation of both *syn*- and *anti*-isomers for the bis-dpmp dinuclear Pt(I) system.

Whereas the diplatinum complexes **1** and **2** are asymmetrical in their crystalline forms, the $^1H$ NMR spectra showed the symmetrical patterns for two terminal isocyanide ligands as mentioned above. Further, the $^{31}P\{^1H\}$ NMR spectra were very broad and featureless, which were invariant from −80 to 50 °C, strongly suggesting a fluxional behavior of dpmp ligands. Plausible fluxional exchanges of two dpmp ligands *via* symmetrical intermediates, *syn*-**1′** and *anti*- **2′**, are depicted in Scheme 2.

**Preparation and Structures of *syn*- and *anti*-$[Pt_2(\mu\text{-dpmp})_2(XylNC)](PF_6)_2$ (3 and 4).** When **1a** was heated at reflux in acetonitrile, *anti*-$[Pt_2(\mu\text{-dpmp})_2(XylNC)](PF_6)_2$ (**4**) was obtained in 56% yield together with the starting complex **1a** (30%) and its isomer **2a** (3%). The similar treatment of **2a** also gave complex **4**. These results implied that an interconversion between

**Scheme 2**

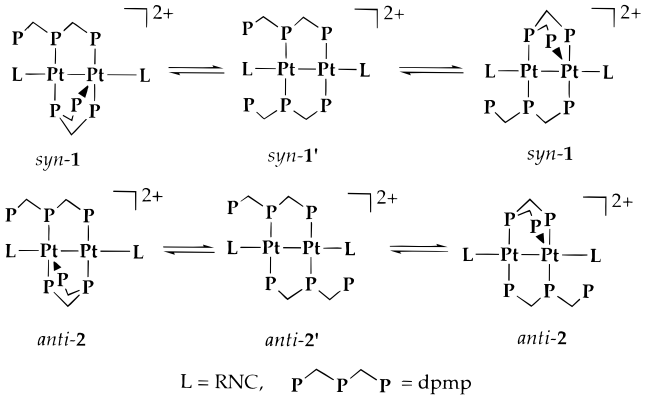


**Scheme 3**

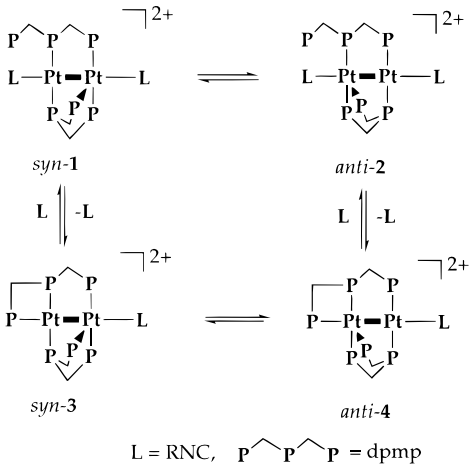


*syn*- and *anti*-arrangements of two dpmp ligands could be promoted at higher temperature (Scheme 3) and **4** might be the most thermodynamically stable compound. Reaction of **1a** with $[Cu^{I}(CH_3CN)_4](PF_6)$ at room temperature exclusively led to a loss of one isocyanide molecule to afford *syn*-$[Pt_2(\mu\text{-dpmp})_2(XylNC)](PF_6)_2$ (**3**) (71%), which was further converted into **4** at reflux in acetonitrile. The structures of **3** and **4** were determined by X-ray crystallography.

A perspective view of the complex cation of **3** with the atomic numbering scheme is shown in Figure 3, and some selected bond lengths and angles are listed in Table 5. The complex cation of **3** consists of four- and five-coordinate platinum atoms asymmetrically bridged by two dpmp ligands. The Pt(2) atom is ligated by three phosphorus atoms of dpmp ligands (P(2), P(3), P(5)) and the adjacent platinum atom (Pt(1)) in a distorted planar geometry, and the Pt(1) atom is coordinated by three phosphorus atoms of dpmp ligands (P(1), P(4), P(6)), one terminal isocyanide (C(1)), and the neighboring platinum atom (Pt(2)). The coordination geometry around the Pt(1) atom is considerably distorted, and the Pt(1)−P(4) distance of 2.446(4) Å is longer than those to other P atoms (2.310(4)−2.346(4) Å). The Pt(1)−Pt(2) distance of 2.6834(8) Å is slightly shorter than is found in **1a** (2.7094(8) Å). Both dpmps act as bridging and chelating ligands in different ways. One dpmp ligand bridges between the two Pt atoms with a pair of terminal and central P atoms (P(1) and P(2)) and chelates to the Pt(2) atom with the other pair (P(2) and P(3)) forming a four-membered ring (P(2)−Pt(1)−P(3) = 72.6(1)°). The other dpmp ligand chelates to the Pt(1) atom with two terminal P atoms (P(4) and P(6)), forming a boat conformation of a six-membered ring, and is bridged to the Pt(2) atom through the central P atom (P(5)). The former coordination mode was observed in $[PtIr(CO)Cl(\mu\text{-dpmp})_2]^{2+}$ and $[PdIr(CO)Cl(\mu\text{-dpmp})_2]^{2+}$,[25] and the latter in *syn*-**1a** and *anti*-**2a** as well as in $[Re_2Cl_3(\mu\text{-dpmp})_2]^{+}$.[24] The complex cation of **4** is an isomer of **3** and is comprised of $PtP_4$ and $PtP_2C$ units joined by a metal−metal single bond (Figure 4 and Table 6). The Pt−Pt distance is 2.7150(7) Å, which is comparable to that of **1a** (2.7094(8) Å) and is slightly longer than those found in **2a** (2.683(2) Å) and **3** (2.6834(8) Å).

The family of bis-dpmp diplatinum(I) complexes (**1**−**4**), having a 32 valence electron count, showed considerably longer Pt−Pt bonds than those of typical Pt(I) dimers having 30 valence electrons.

**Reactions of 1 (*syn*) and 2 (*anti*) with $[M_3(RNC)_6]$ (M = Pt, Pd).** Complexes **1** and **2** could be considered

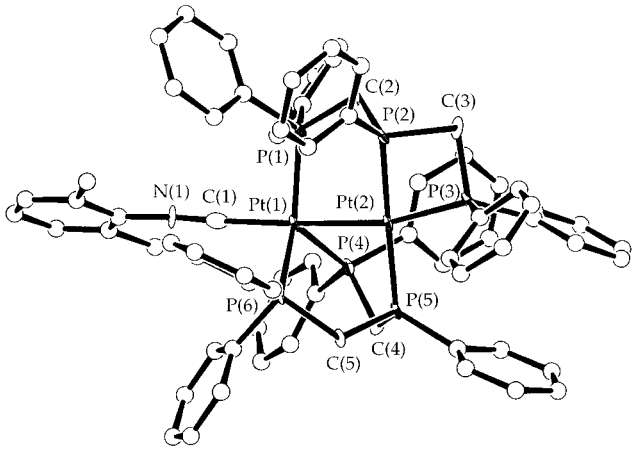


**Figure 3.** ORTEP plot of the complex cation of **3**, *syn*-$[Pt_2(\mu\text{-dpmp})_2(XylNC)](PF_6)_2$. Thermal ellipsoids are drawn at the 30% probability level. The phenyl and xylyl carbon atoms are represented by arbitrary circles, and hydrogen atoms are omitted for clarity.

**Table 5. Selected Bond Lengths (Å) and Angles (deg) of *syn*-$[Pt_2(\mu\text{-dpmp})_2(XylNC)](PF_6)_2$ (3)[a]**

| | | | |
|---|---|---|---|
| **Bond Lengths** | | | |
| Pt(1)−Pt(2) | 2.6834(8) | Pt(1)−P(1) | 2.346(4) |
| Pt(1)−P(4) | 2.446(4) | Pt(1)−P(6) | 2.310(4) |
| Pt(1)−C(1) | 2.00(2) | Pt(2)−P(2) | 2.257(4) |
| Pt(2)−P(3) | 2.273(4) | Pt(2)−P(5) | 2.280(4) |
| N(1)−C(1) | 1.16(2) | N(1)−C(11) | 1.42(2) |
| **Bond Angles** | | | |
| Pt(2)−Pt(1)−P(1) | 88.68(9) | Pt(2)−Pt(1)−P(4) | 84.10(9) |
| Pt(2)−Pt(1)−P(6) | 79.99(9) | Pt(2)−Pt(1)−C(1) | 169.2(4) |
| P(1)−Pt(1)−P(4) | 111.7(1) | P(1)−Pt(1)−P(6) | 145.7(1) |
| P(1)−Pt(1)−C(1) | 89.7(4) | P(4)−Pt(1)−P(6) | 99.3(1) |
| P(4)−Pt(1)−C(1) | 106.4(4) | P(6)−Pt(1)−C(1) | 95.4(4) |
| Pt(1)−Pt(2)−P(2) | 95.4(1) | Pt(1)−Pt(2)−P(3) | 166.5(1) |
| Pt(1)−Pt(2)−P(5) | 86.51(9) | P(2)−Pt(2)−P(3) | 72.6(1) |
| P(2)−Pt(2)−P(5) | 178.0(1) | P(3)−Pt(2)−P(5) | 105.5(1) |
| Pt(1)−P(1)−C(2) | 118.8(5) | Pt(2)−P(2)−C(2) | 110.1(5) |
| Pt(2)−P(2)−C(3) | 94.7(5) | C(2)−P(2)−C(3) | 111.3(6) |
| Pt(2)−P(3)−C(3) | 94.1(5) | Pt(1)−P(4)−C(4) | 106.0(4) |
| Pt(2)−P(5)−C(4) | 116.0(4) | Pt(2)−P(5)−C(5) | 98.7(5) |
| C(4)−P(5)−C(5) | 103.1(6) | Pt(1)−P(6)−C(5) | 116.1(4) |
| C(1)−N(1)−C(11) | 175(1) | Pt(1)−C(1)−N(1) | 177(1) |

[a] Estimated standard deviations are given in parentheses.

(25) Balch, A. L.; Catalano, V. J. *Inorg. Chem.* **1992**, *31*, 2569.

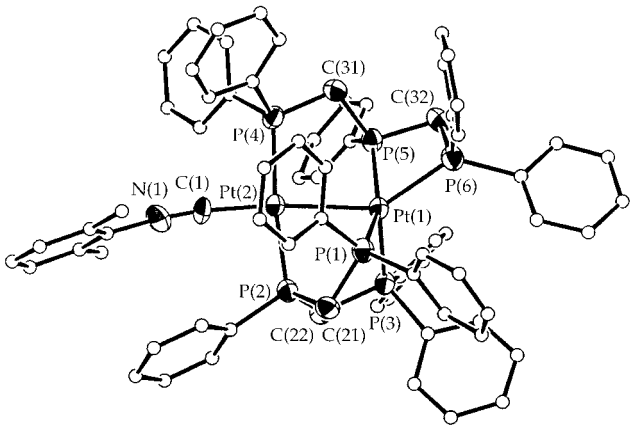


**Figure 4.** ORTEP plot of the complex cation of **4**, *anti*-$[Pt_2(\mu\text{-dpmp})_2(XylNC)](PF_6)_2$. Thermal ellipsoids are drawn at the 40% probability level. The phenyl and xylyl carbon atoms are represented by arbitrary circles, and hydrogen atoms are omitted for clarity.

**Table 6. Selected Bond Lengths (Å) and Angles (deg) of *anti*-$[Pt_2(\mu\text{-dpmp})_2(XylNC)](PF_6)_2$ (4)[a]**

| | | | |
|---|---|---|---|
| Bond Lengths | | | |
| P(t(1)−P(t(2) | 2.7150(7) | P(t(1)−P(1) | 2.314(3) |
| P(t(1)−P(3) | 2.433(3) | P(t(1)−P(5) | 2.267(3) |
| P(t(1)−P(6) | 2.359(3) | P(t(2)−P(2) | 2.291(3) |
| P(t(2)−P(4) | 2.336(3) | P(t(2)−C(1) | 1.92(1) |
| N(1)−C(1) | 1.17(1) | N(1)−C(11) | 1.43(2) |
| Bond Angles | | | |
| Pt(2)−Pt(1)−P(1) | 78.67(8) | Pt(2)−Pt(1)−P(3) | 96.51(7) |
| Pt(2)−Pt(1)−P(5) | 85.52(8) | Pt(2)−Pt(1)−P(6) | 142.60(8) |
| P(1)−Pt(1)−P(3) | 96.1(1) | P(1)−Pt(1)−P(5) | 152.2(1) |
| P(1)−Pt(1)−P(6) | 109.2(1) | P(3)−Pt(1)−P(5) | 108.4(1) |
| P(3)−Pt(1)−P(6) | 118.0(1) | P(5)−Pt(1)−P(6) | 71.0(1) |
| Pt(1)−Pt(2)−P(2) | 80.19(8) | Pt(1)−Pt(2)−P(4) | 92.64(8) |
| Pt(1)−Pt(2)−C(1) | 172.8(4) | P(2)−Pt(2)−P(4) | 171.5(1) |
| P(2)−Pt(2)−C(1) | 93.9(4) | P(4)−Pt(2)−C(1) | 93.6(4) |
| Pt(1)−P(1)−C(21) | 105.9(4) | Pt(2)−P(2)−C(21) | 109.4(4) |
| Pt(2)−P(2)−C(22) | 112.1(4) | C(21)−P(2)−C(22) | 106.1(5) |
| Pt(1)−P(3)−C(22) | 106.3(4) | Pt(2)−P(4)−C(31) | 113.1(4) |
| Pt(1)−P(5)−C(31) | 110.1(4) | Pt(1)−P(5)−C(32) | 97.1(4) |
| C(31)−P(5)−C(32) | 105.5(5) | Pt(1)−P(6)−C(32) | 93.5(4) |
| C(1)−N(1)−C(11) | 174(1) | Pt(2)−C(1)−N(1) | 173(1) |

[a] Estimated standard deviations are given in parentheses.

**Scheme 4**

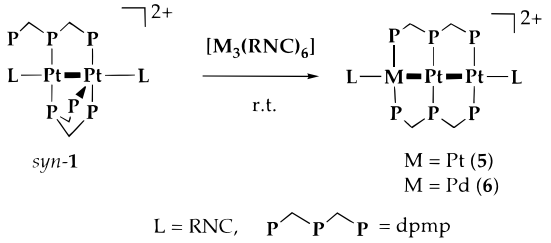


as good precursors of tri- and higher-nuclear clusters since they possess pendant arm phosphine units in solution. In this regard, we have tried their reaction with zerovalent platinum and palladium complexes of isocyanide, $[M_3(RNC)_6]$ (M = Pt, Pd), which are good precursors of the $d^{10}$ $M(RNC)_2$ fragment.

Reaction of *syn*-$[Pt_2(\mu\text{-dpmp})_2(XylNC)_2](PF_6)_2$ (**1a**) with $[Pt_3(XylNC)_6]$ at room temperature yielded orange crystals of *linear*-$[Pt_3(\mu\text{-dpmp})_2(XylNC)_2](PF_6)_2$ (**5**) in a remarkably high yield (Scheme 4). The $^1H$ and $^{13}C$ NMR spectra indicated the presence of one kind of isocyanide ligand, which were further shown to be

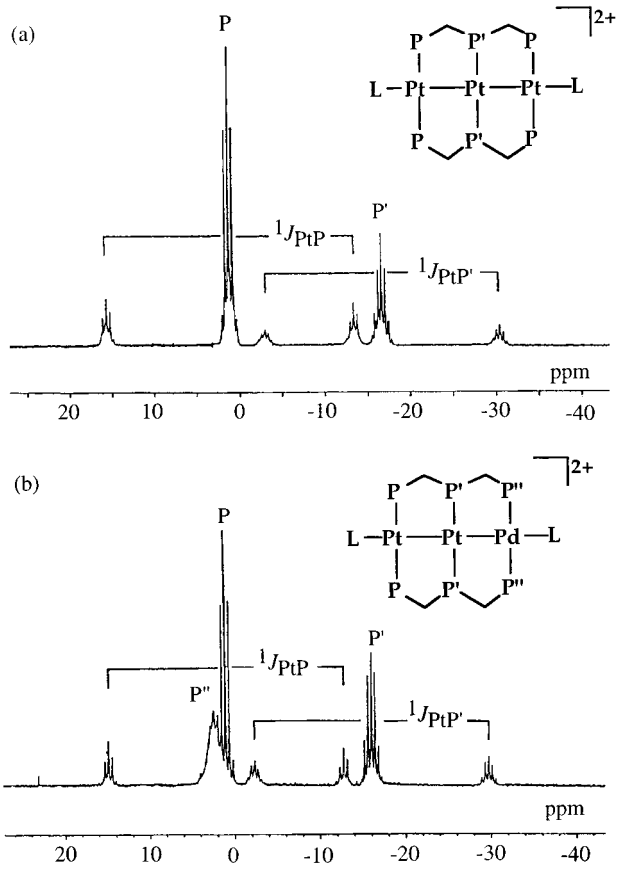


**Figure 5.** $^{31}P\{^1H\}$ NMR spectra of (a) **5** and (b) **6** in acetone-$d_6$ at room temperature and their assignments.

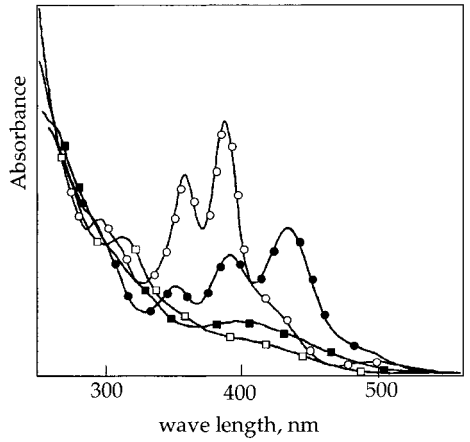


**Figure 6.** Electronic absorption spectra of (a) **5** (−○−), (b) **6** (−●−), (c) **7** (−□−), and (d) **8** (−■−) in dichloromethane.

terminally coordinated to the Pt(I) center by the IR spectrum ($\nu$(N≡C) 2130 $cm^{-1}$). In the $^{31}P\{^1H\}$ NMR spectrum, two sets of resonances centered at −16.8 and 1.1 ppm were observed in an integration ratio of 2:1, both of which were accompanied by satellite peaks due to coupling to $^{195}Pt$ with $^1J_{PtP}$ = 2777 and 2946 Hz (Figure 5a). These spectral features suggested that the dpmp ligands are equivalent and symmetrically bridge a triplatinum core. The electronic absorption spectrum (Figure 6) exhibited intense bands around 389 nm (log $\epsilon$ = 4.13) and 360 nm (4.02) which are characteristic for linearly ordered triplatinum complexes joined by metal−metal $\sigma$-bonds as observed in [{Pt(dppe)(Xyl-

**Scheme 5**

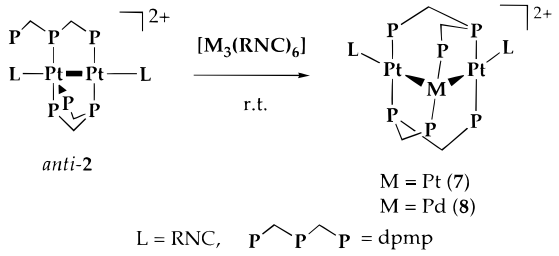


NC)}$_2$Pt(XylNC)$_2$](PF$_6$)$_2$ (408 nm (log $\epsilon$ = 4.14) and 374 nm (3.89)).[3f] The similar reaction of **1a** with [Pd$_3$(XylNC)$_6$] afforded dark orange crystals of the heterotrinuclear complex formulated as *linear*-[Pt$_2$Pd($\mu$-dpmp)$_2$(XylNC)$_2$](PF$_6$)$_2$ (**6**) in 63% yield. The $^1$H and $^{13}$C NMR spectra indicated the presence of two environmentally different isocyanide ligands. In the $^{31}$P{$^1$H} NMR spectrum (Figure 5b), three sets of resonances centered at −16.1, 1.1, and 2.4 ppm were observed in a ratio of 1:1:1, namely the three phosphorus atoms of dpmp sitting in chemically inequivalent circumstances. The former two resonances are accompanied by $^{195}$Pt satellite peaks with $^1J_{PtP}$ = 2774 and 2802 Hz, corresponding to P atoms coordinated to Pt centers. The latter peak ($\delta$ 2.4) is rather broad and is not accompanied by $^{195}$Pt satellite peaks, probably ascribable to P atoms bound to Pd center. In the UV−vis spectrum, the band maxima (435 nm (log $\epsilon$ = 3.98), 393 nm (3.89), and 351 nm (3.76)) considerably shifted to lower energy compared with the Pt$_3$ cluster **5**, whereas the spectral pattern is similar to that of **5** (Figure 6).

When *anti*-[Pt$_2$($\mu$-dpmp)$_2$(RNC)$_2$](PF$_6$)$_2$ (**2a**, R = Xyl) was treated with [Pt$_3$(RNC)$_6$] at room temperature, a yellow cluster formulated as *A-frame*-[Pt$_3$($\mu$-dpmp)$_2$(RNC)$_2$](PF$_6$)$_2$ (**7**, R = Xyl) was obtained in 70% yield (Scheme 5). The IR and $^1$H NMR spectra indicated one kind of terminal isocyanide ligand. The $^{31}$P{$^1$H} NMR spectrum of **7** exhibited three resonances at $\delta$ −34.0, 1.9, and 23.0 in an intensity ratio of 1:1:1, all being accompanied by satellite peaks due to coupling to $^{195}$Pt with $^1J_{PtP}$ = 2581−2900 Hz (Figure 7a). The two resonances at $\delta$ −34.0 and 23.0, in addition, are coupled to each other with $^2J_{PP'}$ = 412 Hz. These spectral data suggested that the three phosphorus atoms of dpmp are in three environmentally different sites around a symmetrical triplatinum aggregation. The electronic absorption is somewhat featureless (Figure 6) and is close to that of [Pt$_3$($\mu$-dppm)$_2$(XylNC)$_4$](PF$_6$)$_2$ (**10**),[3b] which has an A-frame triplatinum structure. The similar treatment of *anti*-[Pt$_2$($\mu$-dpmp)$_2$(RNC)$_2$](PF$_6$)$_2$ (**2b**, R = Mes) with [Pd$_3$(MesNC)$_6$] afforded a heterotrimetallic cluster, *A-frame*-[Pt$_2$Pd($\mu$-dpmp)$_2$(MesNC)$_2$](PF$_6$)$_2$ (**8**) in 31% yield. The IR and $^1$H NMR spectra were similar to those of **7**, whereas a new band appeared at a longer wavelength (396 nm) than that of **7** in the electronic absorption spectrum (Figure 6). The $^{31}$P{$^1$H} NMR spectrum showed the presence of three nonequivalent phosphorus atoms at $\delta$ −29.8, −10.2, and 16.2 (Figure 7b). The spectral pattern was quite similar to that of **7** except the fact that the central peak ($\delta$ −10.2) did not have satellites due to one-bond coupling to $^{195}$Pt.

**Structures of *linear*-[Pt$_2$M($\mu$-dpmp)$_2$(RNC)$_2$](PF$_6$)$_2$ (5, M = Pt; 6, M = Pd).** The structures of **5** and **6** were determined by X-ray crystallography. The complex

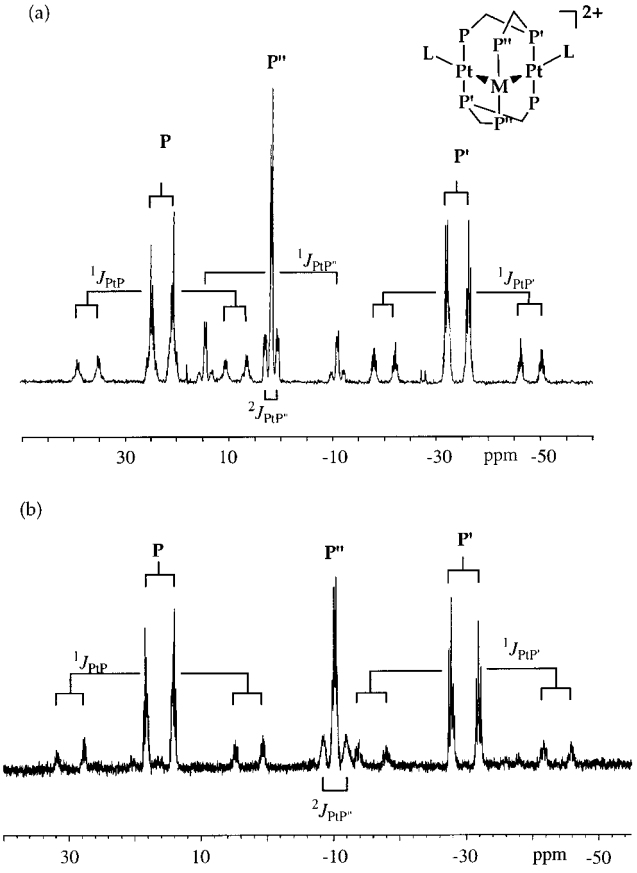


**Figure 7.** $^{31}$P{$^1$H} NMR spectra of (a) **7** and (b) **8** in acetone-$d_6$ at room temperarure and their assignments.

cation of **5** has a pseudo inversion center and is composed of a linear triplatinum structure symmetrically bridged by two dpmp ligands (Figure 8a). The Pt(1)−Pt(2) and Pt(2)−Pt(3) bond lengths are 2.723(2) and 2.724(2) Å, significantly longer than those of the dppm-bridged dimer [Pt$_2$($\mu$-dppm)$_2$Cl$_2$] (2.652 Å)[26] and the unbridged trinuclear complex [Pt$_3$(dppen)$_2$(RNC)$_4$]$^{2+}$ (2.655 Å),[3f] but still demonstrated the presence of covalent bonds between them (Table 7). The L−Pt−Pt−Pt−L core is almost linear with Pt(1)−Pt(2)−Pt(3) = 178.66(8)°, Pt(2)−Pt(1)−C(1) = 172.2(8)°, and Pt(2)−Pt(3)−C(2) = 173.9(7)°. The two dpmp ligands symmetrically support the trinuclear core to produce the *trans*-[Pt**P**$_2$(RNC)], *trans*-[Pt**P**$_2$], and *trans*-[Pt**P**$_2$(RNC)] fragments connected by metal−metal bonds. The three square-planar coordination planes around the Pt atoms are somewhat twisted with the dihedral angles of 34 and 29° between the Pt(1) and Pt(2) planes and the Pt(2) and Pt(3) planes, respectively. The *cis*-PPtPtP torsion angles are within the range of 33.3(3)−39.9(3)°. On the basis of the centrosymmetrical structure of **5**, the apparent oxidation state of the three Pt atoms is estimated as Pt(I)−Pt(0)−Pt(I). The similar trinuclear framework was observed in [Au$_3$(dpmp)$_2$]$^{3+}$ [6] and [Rh$_3$(dpmp)$_2$Cl$_2$(CO)$_3$]$^+$,[5] but there is no direct bonding interaction between Au$^I$ or Rh$^I$ ions. This is the first example of the metal−metal-bonded side-by-side linear triplatinum cluster, the reactivity of which is of remarkable interest in comparison with those of the dppm-bridged diplatinum complexes.[1,27]

(26) Manojlovic-Muir, L. J.; Muir, K. M.; Salomun, T. *Acta Crystallogr.* **1979**, *B35*, 1237.

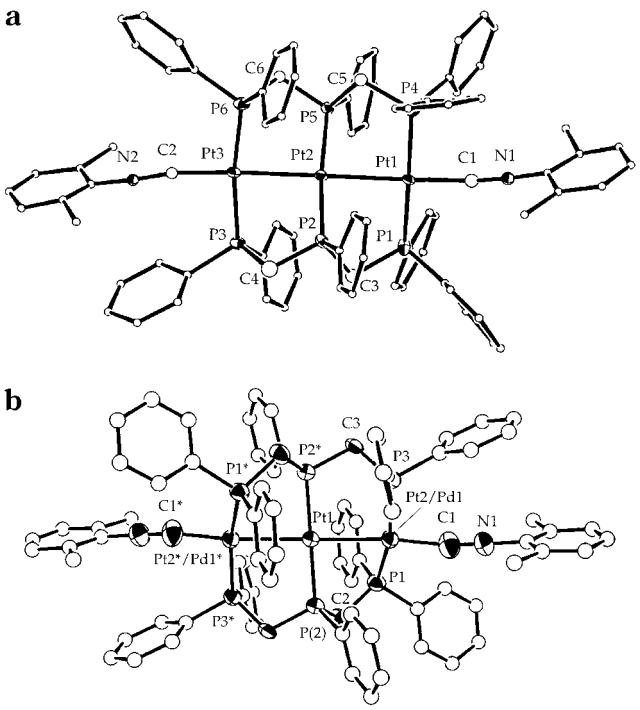


**Figure 8.** ORTEP diagrams of the complex cation of **5**, *linear*-$[Pt_3(\mu\text{-dpmp})_2(XylNC)_2]^{2+}$ (a), and that of **6**, *linear*-$[Pt_2Pd(\mu\text{-dpmp})_2(XylNC)_2]^{2+}$ (b). Thermal ellipsoids are drawn at the 30% (**5**) and 40% (**6**) probability levels. The phenyl and xylyl groups are represented by arbitrary circles, and hydrogen atoms are omitted for clarity.

**Table 7. Selected Bond Lengths (Å) and Angles (deg) of *linear*-$[Pt_3(\mu\text{-dpmp})_2(XylNC)_2](PF_6)_2$ (5)[a]**

| Bond Lengths | | | |
|---|---|---|---|
| Pt(1)−Pt(2) | 2.723(2) | Pt(1)−P(1) | 2.268(9) |
| Pt(1)−P(4) | 2.302(8) | Pt(1)−C(1) | 1.99(3) |
| Pt(2)−Pt(3) | 2.724(2) | Pt(2)−P(2) | 2.235(9) |
| Pt(2)−P(5) | 2.264(8) | Pt(3)−P(3) | 2.313(8) |
| Pt(3)−P(6) | 2.261(8) | Pt(3)−C(2) | 1.93(2) |
| N(1)−C(1) | 1.21(3) | N(1)−C(11) | 1.30(3) |
| N(2)−C(2) | 1.25(3) | N(2)−C(21) | 1.36(3) |
| **Bond Angles** | | | |
| Pt(2)−Pt(1)−P(1) | 88.4(2) | Pt(2)−Pt(1)−P(4) | 90.0(2) |
| Pt(2)−Pt(1)−C(1) | 172.2(8) | P(1)−Pt(1)−P(4) | 175.0(3) |
| P(1)−Pt(1)−C(1) | 95.5(8) | P(4)−Pt(1)−C(1) | 86.6(8) |
| Pt(1)−Pt(2)−Pt(3) | 178.66(8) | Pt(1)−Pt(2)−P(2) | 86.0(2) |
| Pt(1)−Pt(2)−P(5) | 88.2(2) | Pt(3)−Pt(2)−P(2) | 93.2(2) |
| Pt(3)−Pt(2)−P(5) | 92.6(2) | P(2)−Pt(2)−P(5) | 174.0(3) |
| Pt(2)−Pt(3)−P(3) | 84.7(2) | Pt(2)−Pt(3)−P(6) | 85.6(2) |
| Pt(2)−Pt(3)−C(2) | 173.9(7) | P(3)−Pt(3)−P(6) | 170.1(3) |
| P(3)−Pt(3)−C(2) | 91.1(8) | P(6)−Pt(3)−C(2) | 98.7(8) |
| Pt(1)−P(1)−C(3) | 116(1) | Pt(2)−P(2)−C(3) | 112(1) |
| Pt(2)−P(2)−C(4) | 116(1) | C(3)−P(2)−C(4) | 101(1) |
| Pt(3)−P(3)−C(4) | 108(1) | Pt(1)−P(4)−C(5) | 115(1) |
| Pt(2)−P(5)−C(5) | 108.2(9) | Pt(2)−P(5)−C(6) | 116.5(9) |
| C(5)−P(5)−C(6) | 100(1) | Pt(3)−P(6)−C(6) | 110.2(9) |
| C(1)−N(1)−C(11) | 175(3) | C(2)−N(2)−C(21) | 174(3) |
| Pt(1)−C(1)−N(1) | 168(2) | Pt(3)−C(2)−N(2) | 169(2) |

[a] Estimated standard deviations are given in parentheses.

The structure of complex **6** is isostructural with **5** (Figure 8b), the Pd atoms occupying the terminal position which is consistent with the $^{31}P\{^1H\}$ NMR spectrum. The crystal structure of the complex cation has an inversion center and is refined with a disordered model in which the terminal metal site is occupied by a Pt atom with 0.5 multiplicity and a Pd atom with 0.5 multiplicity. That is, the Pt−Pt−Pd and Pd−Pt−Pt structures are averaged. The average metal−metal bond length is 2.690(1) Å, which is shorter than the Pt−Pt distances in **5** due to an incorporation of a palladium atom into the cluster core (Table 8). The covalent radius of Pd is smaller than those of Pt, and indeed, between the analogous dimetal complexes, $[Pt_2(dppp)_2(MesNC)_2]^{2+}$ [3f] and $[Pd_2(dppp)_2(MesNC)_2]^{2+}$,[3e] the Pd(I)−Pd(I) bond length (2.617(2) Å) is shorter by 0.036 Å than the Pt(I)−Pt(I) one (2.653(1) Å). The structure of **6** with the asymmetrical Pt−Pt−Pd structure clearly indicated a mechanism where the $d^{10}$ $M(RNC)_2$ fragment is trapped by the two uncoordinated P atoms of **1′** to sit in a terminal position of the trinuclear array, followed by formation of a metal−metal bond and a dissociation of the isocyanide ligands. One electron transfer from the terminal Pd atom to the central Pt atom resulted in a formation of Pt(I)−Pt(0)−Pd(I) cluster core. The mechanistic aspect is quite different in comparison with that for the A-frame triplatinum cluster (*vide infra*).

**Table 8. Selected Bond Lengths (Å) and Angles (deg) of *linear*-$[Pt_2Pd(\mu\text{-dpmp})_2(XylNC)_2](PF_6)_2$ (6)[a,b]**

| Bond Lengths | | | |
|---|---|---|---|
| Pt(1)−M | 2.690(1) | Pt(1)−M* | 2.690(1) |
| Pt(1)−P(2) | 2.262(2) | Pt(1)−P(2)* | 2.262(2) |
| M−P(1) | 2.294(2) | M−P(3) | 2.293(3) |
| M−C(1) | 1.992(9) | N(1)−C(1) | 1.17(1) |
| N(1)−C(11) | 1.43(1) | | |
| **Bond Angles** | | | |
| M−Pt(1)−M* | 180.00 | M−Pt(1)−P(2) | 85.93(7) |
| M−Pt(1)−P(2)* | 94.07(7) | M−Pt(1)−P(2) | 94.07(7) |
| M−Pt(1)−P(2)* | 85.93(7) | P(2)−Pt(1)−P(2)* | 180.00 |
| Pt(1)−M−P(1) | 84.80(8) | Pt(1)−M−P(3) | 87.02(7) |
| Pt(1)−M−C(1) | 166.9(3) | P(1)−M−P(3) | 160.55(8) |
| P(1)−M−C(1) | 99.8(2) | P(3)−M−C(1) | 92.1(3) |
| M−P(1)−C(2) | 115.6(2) | Pt(1)−P(2)−C(2) | 109.9(3) |
| Pt(1)−P(2)−C(3) | 114.4(2) | C(2)−P(2)−C(3) | 103.8(3) |
| M−P(3)−C(3) | 110.1(2) | C(1)−N(1)−C(11) | 176.6(9) |
| M−C(1)−N(1) | 168.2(7) | | |

[a] Estimated standard deviations are given in parentheses. [b] M = Pt(2) and Pd(1) with 0.5 occupancies. Asterisks indicate equivalent atom positions.

**Structures of *A-frame*-$[Pt_2M(\mu\text{-dpmp})_2(RNC)_2](PF_6)_2$ (7, M = Pt; 8, M = Pd).** An X-ray crystallographic analysis revealed that complex **7** comprises an A-frame triplatinum core bridged by two dpmp ligands as shown in Figure 9a. The complex cation has a crystallographically imposed $C_2$ symmetry. The core geometry is quite similar to that of $[Pt_3(\mu\text{-dppm})_2(XylNC)_4](PF_6)_2$ (**10**) except for the geometry around the central Pt atom, which is fairly distorted from a square planar structure. The dihedral angle between the planes [Pt(1)Pt(2)Pt(2)*] and [Pt(1)P(3)P(3)*] is 16°. The dpmp ligand bridges over the Pt(2) and Pt(2)* atoms with a pair of the outer and inner P atoms and between the Pt(1) and Pt(2) atoms with the other pair. The double bridging system of dpmp results in thermal stability of complex **7**. The Pt(1)−Pt(2) bond distance is 2.6309(7) Å, and the interatomic Pt(2)···Pt(2)* distance is 3.2333(9) Å (Table 9). The former corresponds to a Pt−Pt $\sigma$-bond, and the latter indicates the absence of bonding interaction between the two terminal Pt atoms. The Pt(1)−Pt(2)−Pt(1)* angles is 76.76(3)°. The structure of **8** was also confirmed by X-ray crystallography to have a symmetrical $Pt_2Pd$ A-frame assembly

(27) Tanase, T.; Ukaji, H.; Igoshi, T.; Yamamoto, Y. *Inorg. Chem.* **1996**, *35*, 4114.

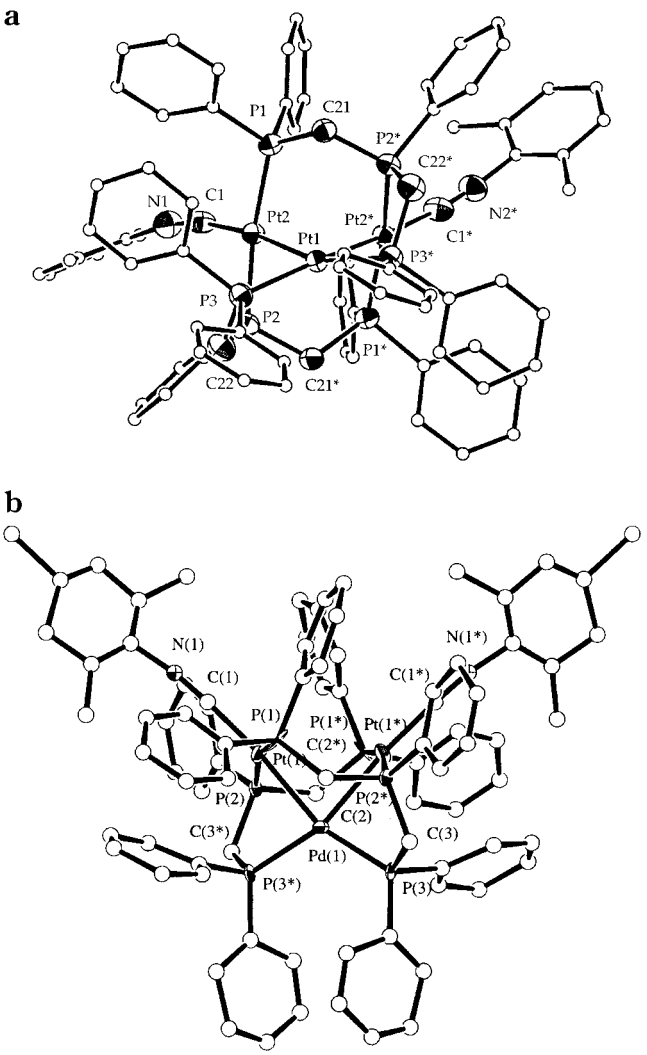


**Figure 9.** ORTEP diagrams of the complex cation of **7**, *A-frame*-$[Pt_3(\mu\text{-dpmp})_2(XylNC)_2]^{2+}$ (a), and that of **8**, *A-frame*-$[Pt_2Pd(\mu\text{-dpmp})_2(XylNC)_2]^{2+}$ (b). Thermal ellipsoids are drawn at the 40% (**7**) and 30% (**8**) probability levels. The phenyl and xylyl groups are represented by arbitrary circles, and hydrogen atoms are omitted for clarity.

**Table 9. Selected Bond Lengths (Å) and Angles (deg) of *A-frame*-$[Pt_3(\mu\text{-dpmp})_2(XylNC)_2](PF_6)_2$ (7)[a]**

| Bond Lengths | | | |
|---|---|---|---|
| Pt(1)−Pt(2) | 2.6039(7) | Pt(1)−P(3) | 2.268(3) |
| Pt(1)−P(3)* | 2.268(3) | Pt(2)−P(1) | 2.322(3) |
| Pt(2)−P(2) | 2.274(3) | Pt(2)−C(1) | 1.96(1) |
| N(1)−C(1) | 1.15(1) | N(1)−C(11) | 1.42(1) |

| Bond Angles | | | |
|---|---|---|---|
| Pt(2)−Pt(1)−Pt(2)* | 76.76(3) | Pt(2)−Pt(1)−P(3) | 84.63(8) |
| Pt(2)−Pt(1)−P(3)* | 156.97(8) | Pt(2)*−Pt(1)−P(3) | 156.97(8) |
| Pt(2)*−Pt(1)−P(3)* | 84.63(8) | P(3)−Pt(1)−P(3)* | 116.4(2) |
| Pt(1)−Pt(2)−P(1) | 88.53(7) | Pt(1)−Pt(2)−P(2) | 76.57(7) |
| Pt(1)−Pt(2)−C(1) | 172.3(3) | P(1)−Pt(2)−P(2) | 164.8(1) |
| P(1)−Pt(2)−C(1) | 98.6(3) | P(2)−Pt(2)−C(1) | 96.1(3) |
| Pt(2)−P(1)−C(21) | 117.6(3) | Pt(2)−P(2)−C(21) | 114.3(3) |
| Pt(2)−P(2)−C(22) | 109.8(4) | C(21)−P(2)−C(22) | 106.0(5) |
| Pt(1)−P(3)−C(22) | 101.9(4) | C(1)−N(1)−C(11) | 167(1) |
| Pt(2)−C(1)−N(1) | 169(1) | | |

[a] Estimated standard deviations are given in parentheses. Asterisks indicate equivalent atom positions.

(Figure 9b). The Pd atom is ordered and occupies the central position between the two Pt atoms. The Pt(1)−Pd(1) bond length of 2.599(3) Å is shorter by 0.031 Å than the Pt−Pt bond length of **7**, and the Pt(1)···Pt(1)* interatomic distance of 3.290(3) Å is out of bonding range (Table 10). The Pt(1)−Pd(1)−Pt(1)* angles are 78.5(1)°.

**Table 10. Selected Bond Lengths (Å) and Angles (deg) of *A-frame*-$[Pt_2Pd(\mu\text{-dpmp})_2(XylNC)_2](PF_6)_2$ (8)[a]**

| Bond Lengths | | | |
|---|---|---|---|
| Pt(1)−Pd(1) | 2.599(3) | Pt(1)−P(1) | 2.323(8) |
| Pt(1)−P(2) | 2.274(8) | Pt(1)−C(1) | 1.97(3) |
| Pd(1)−P(3) | 2.298(8) | Pd(1)−P(3)* | 2.298(8) |
| N(1)−C(1) | 1.19(3) | N(1)−C(11) | 1.43(4) |

| Bond Angles | | | |
|---|---|---|---|
| Pd(1)−Pt(1)−P(1) | 86.0(2) | Pd(1)−Pt(1)−P(2) | 75.5(2) |
| Pd(1)−Pt(1)−C(1) | 173.3(8) | P(1)−Pt(1)−P(2) | 161.3(3) |
| P(1)−Pt(1)−C(1) | 98.7(9) | P(2)−Pt(1)−C(1) | 99.5(9) |
| Pt(1)−Pd(1)−Pt(1)* | 78.5(1) | Pt(1)−Pd(1)−P(3) | 158.7(2) |
| Pt(1)−Pd(1)−P(3)* | 84.0(2) | Pt(1)*−Pd(1)−P(3) | 84.0(2) |
| Pt(1)*−Pd(1)−P(3)* | 158.7(2) | P(3)−Pd(1)−P(3)* | 115.4(4) |
| Pt(1)−P(1)−C(2)* | 118.9(9) | Pt(1)−P(2)−C(2) | 114.8(9) |
| Pt(1)−P(2)−C(3)* | 109(1) | C(2)−P(2)−C(3)* | 106(1) |
| Pd(1)−P(3)−C(3) | 102(1) | C(1)−N(1)−C(11) | 172(3) |
| Pt(1)−C(1)−N(1) | 177(3) | | |

[a] Estimated standard deviations are given in parentheses. Asterisks indicate equivalent atom positions.

The structure of **8** suggests a formation mechanism which involves an insertion of $d^{10}$ $M(RNC)_2$ fragment into the Pt−Pt bond in **2′** supported by the ligation of the two uncoordinated P atoms. Since Hoffmann et al. theoretically predicted the existence of A-frame trinuclear complexes on the basis of the isolobal analogy between $CH_2$ and $d^{10}$ $ML_2$ and $d^8$ $ML_4$ fragments,[28] several synthetic examples have been prepared through insertion of metal fragments into Pd−Pd and Pt−Pt $\sigma$-bonds bridged by diphosphines such as dppm (bis(diphenylphosphino)methane) and dmpm (bis(dimethylphosphino)methane). The A-frame triplatinum cluster $[Pt_2(\mu\text{-}PtL_2)(\mu\text{-dppm})_2L_2]^{2+}$ (L = isocyanide)[3b] was prepared by the metal fragment ($ML_2$) insertion into the Pt−Pt bond of $[Pt_2(\mu\text{-dppm})_2L_2]^{2+}$, and the heterotrimetallic A-frame clusters $[Pt_2(\mu\text{-}HgCl_2)Cl_2(\mu\text{-dppm})_2]$[29] and $[Pt_2(\mu\text{-AuI})(C_2tBu)_2(\mu\text{-dppm})_2]$[30] have been prepared by the reactions of the dppm-bridged diplatinum complexes with $HgCl_2$ and AuI, respectively. The reaction of $[Pd_2Cl_2(dmpm)_2]$ with $[Pt(PPh_3)_2(C_2H_4)]$ also led to the heterometallic cluster $[Pd_2(\mu\text{-}Pt(PPh_3)_2)Cl_2(\mu\text{-dmpm})_2]$.[31] On the basis of these examples, the formation of **8** from **2** can be accommodated within the context of an insertion of $d^{10}$ $ML_2$ fragment into the metal−metal $\sigma$-bond. An insertion of $Pd(XylNC)_2$ fragment into the Pt(I)−Pt(I) $\sigma$-bond is followed by an displacement of isocyanide ligands with the terminal phosphine units. The structure of **2** having two pendant arms of the phosphine unites is estimated to play a key role, since the nonbridged dimer $[Pt_2(dppp)_2(RNC)_2]^{2+}$ hardly underwent the insertion of a $M(RNC)_2$ fragment (M = Pt, Pd). Furthermore, the appropriately arranged uncoordinated phosphorus atoms in *anti*-**2** may accelerate the insertion. The position of the trapped metal atom in **8** (central position) is interestingly contrasted with that in *linear*-$[Pt_2Pd(\mu\text{-dpmp})_2(XylNC)_2]^{2+}$ (**6**) derived from the reaction of *syn*-$[Pt_2(\mu\text{-dpmp})_2(XylNC)_2]^{2+}$ (**1a**) with

(28) Hoffman, D. M.; Hoffmann, R. *Inorg. Chem.* **1981**, *20*, 3543.
(29) Sharp, P. R. *Inorg. Chem.* **1986**, *25*, 4185.
(30) Manojlovic-Muir, L.; Muir, K. W.; Treurnicht, I.; Puddephatt, R. J. *Inorg. Chem.* **1987**, *26*, 2418.
(31) Ni, J.; Kubiak, C. P. *Inorg. Chim. Acta* **1987**, *127*, L37.

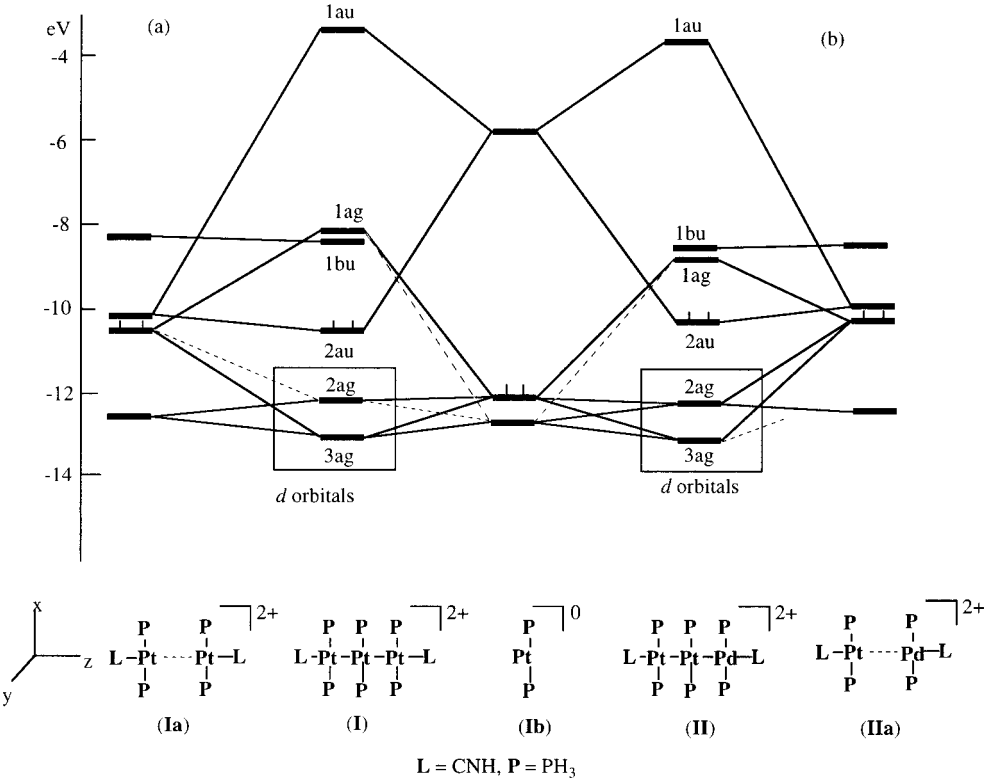


**Figure 10.** MO interaction diagrams for (a) *linear*-$[Pt_3(PH_3)_6(HNC)_2]^{2+}$ (**I**) in terms of $[(CNH)(PH_3)_2Pt\cdots Pt(PH_3)_2(CNH)]^{2+}$ (**Ia**) and $[Pt(PH_3)_2]$ (**Ib**) fragments and for (b) *linear*-$[Pt_2Pd(PH_3)_6(HNC)_2]^{2+}$ (**II**) in terms of $[(CNH)(PH_3)_2Pt\cdots Pd(PH_3)_2(CNH)]^{2+}$ (**IIa**) and $[Pt(PH_3)_2]$ (**Ib**) fragments.

the $Pd(XylNC)_2$ fragment (terminal position). The arrangement of the two free phosphorus atoms in **1′** and **2′** may play a critical role in determining the direction of the $d^{10}$ metal-inserted position.

**Molecular Orbital Calculations.** In order to elucidate and compare the electronic structures of metal−metal bonds in the homo- and heterotrinuclear complexes **5**−**8**, extended Hückel molecular orbital calculations were carried out on the model systems *linear*-$[Pt_3(PH_3)_6(CNH)_2]^{2+}$ (**I**), *linear*-$[Pt_2Pd(PH_3)_6(CNH)_2]^{2+}$ (**II**), *A-frame*-$[Pt_3(PH_3)_6(CNH)_2]^{2+}$ (**III**), and *A-frame*-$[Pt_2Pd(PH_3)_6(CNH)_2]^{2+}$ (**IV**) together with related models $[Pt_2(PH_3)_4(CNH)_2]^{2+}$ (**V**) and *A-frame*-$[\{trans\text{-}Pt(PH_3)_2(CNH)\}_2\{cis\text{-}Pt(CNH)_2\}]^{2+}$ (**VI**).

An interaction diagram of **I** in terms of $[(HNC)(PH_3)_2Pt^{I}\cdots Pt^{I}(PH_3)_2(CNH)]^{2+}$ (fragment **Ia**) and $Pt^0(PH_3)_2$ (fragment **Ib**) is shown in Figure 10a. The model compound **I** possesses a $C_{2h}$ symmetry with respect to the *z* axis, where all P−Pt−Pt−P torsion angles are 0 or 180° and the L−Pt−Pt−Pt−L core is linear. The LUMO of **Ia** interacts with the LUMO of **Ib** to generate $\sigma$-bonding ($2a_u$) and $\sigma$-antibonding ($1a_u$) orbitals. The former ($2a_u$) is occupied by two electrons and consists of the hybridized orbitals of the outer Pt atoms ($p_z$, $d_{x^2-y^2}$, $d_{z^2}$) and the $p_z$ orbital of the central Pt atom. The HOMO of **Ia** also strongly interacts with the HOMO of **Ib** producing filled bonding ($3a_g$) and empty antibonding ($1a_g$) orbitals. The low-lying d orbitals of fragments **Ia** and **Ib** are mixed into the former one. The $3a_g$ orbital mainly consists of $p_z$ and $d_{z^2}$ orbitals of the outer Pt atoms and $d_{x^2-y^2}$ and $d_{z^2}$ orbitals of the central Pt atom. These two significant interactions suggest that the three Pt atoms are joined by two covalent bonds although the observed Pt−Pt bond length is relatively long. Another

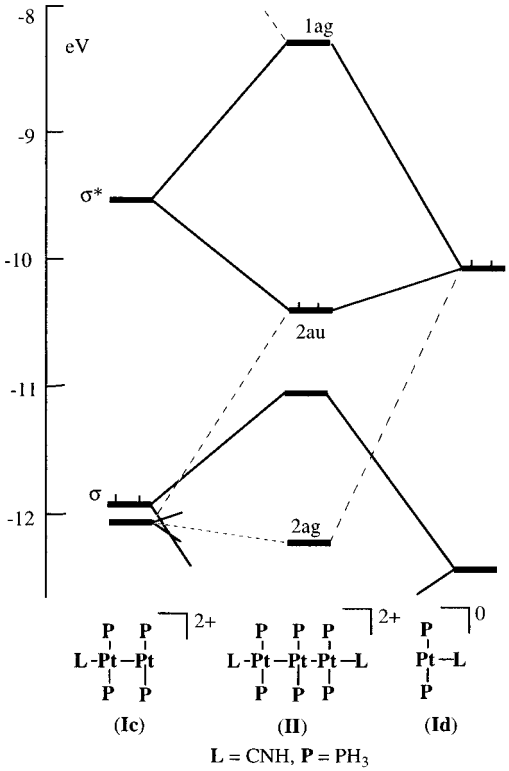


**Figure 11.** MO interaction diagram for *linear*-$[Pt_3(PH_3)_6(HNC)_2]^{2+}$ (**I**) in terms of $[Pt_2(PH_3)_4(HNC)]^{2+}$ (**Ic**) and $[Pt(PH_3)_2(HNC)]$ (**Id**) fragments.

interaction diagram for **I** in terms of $[Pt^{I}_2(PH_3)_2(CNH)]^{2+}$ (**Ic**) and $Pt^0(PH_3)_2(CNH)$ (**Id**) is illustrated in Figure 11. A conspicuous interaction between the LUMO of **Ic** having Pt−Pt $\sigma$-bonding character and the

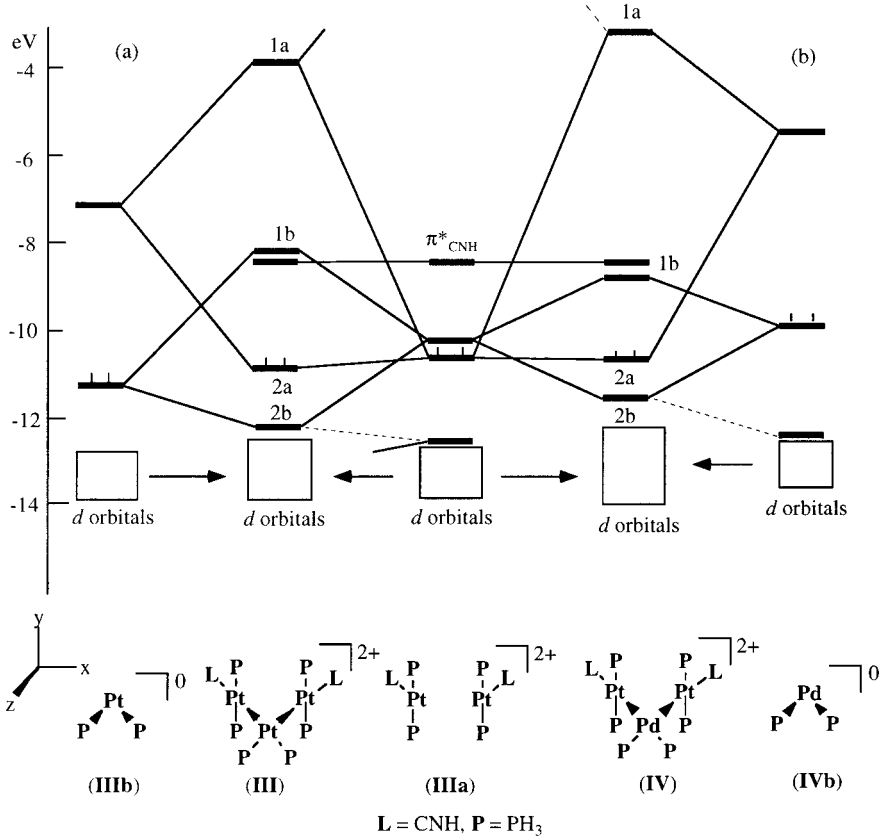


**Figure 12.** MO interaction diagrams for (a) *A-frame*-$[Pt_3(PH_3)_6(HNC)_2]^{2+}$ (**III**) in terms of $[(CNH)(PH_3)_2Pt\cdots Pt(PH_3)_2(CNH)]^{2+}$ (**IIIa**) and $[Pt(PH_3)_2]$ (**IIIb**) fragments and for (b) *A-frame*-$[Pt_2Pd(PH_3)_6(HNC)_2]^{2+}$ (**IV**) in terms of $[(CNH)(PH_3)_2Pt\cdots Pt(PH_3)_2(CNH)]^{2+}$ (**IIIa**) and $[Pd(PH_3)_2]$ (**IVb**) fragments.

HOMO of **Id** generates a filled bonding orbital ($2a_u$) and an unoccupied antibonding one ($1a_g$). This scheme clearly demonstrates that one electron is transferred from the terminal Pt atom to the central one after the $d^{10}$ $Pt^0$ species is trapped into the terminal site of the $Pt_3$ core, which is also evident in the net charge population of **I**, that of the terminal Pt being −0.50 and that of the central Pt being −0.75. The HOMO−LUMO energy gap of **I** is 2.15 eV, which is remarkably smaller than that (3.01 eV) of $[Pt_2(PH_3)_4(CNH)_2]^{2+}$ (**V**), a model for $[Pt_2(\mu\text{-dppm})_2(RNC)_2]^{2+}$. The higher energy level of the HOMO of **I** is ascribable to the smaller HOMO−LUMO gap. In other words, the triplatinum core of **5** is estimated to be more nucleophilic than the diplatinum core of **9**. The MO profiles of *linear*-$[Pt_2Pd(PH_3)_6(CNH)_2]^{2+}$ (**II**) are similar to those of **I** except for the higher energy of the HOMO and smaller HOMO−LUMO gap (1.76 eV) (Figure 10b).

An interaction diagram of **III** in terms of $[(HNC)(PH_3)_2Pt^I\cdots Pt^I(PH_3)_2(CNH)]^{2+}$ (fragment **IIIa**) and $Pt^0(PH_3)_2$ (fragment **IIIb**) is shown in Figure 12a. The model compound **III** possesses a $C_2$ symmetry with respect to the *z* axis. The diagram clearly shows that three Pt atoms are connected by two covalent bonds as reported for **VI**.[3b] The HOMO is significantly stabilized by ∼0.33 eV (HOMO−LUMO gap = 2.50 eV) in comparison with the linear trinuclear model **I**. When the central Pt is replaced by Pd (**IV**), the HOMO−LUMO gap becomes smaller (1.84 eV) as observed in model **II**.

**Conclusion.** The present reactions of dinuclear platinum complexes *syn*-**1** and *anti*-**2** with the $d^{10}$ $ML_2$ fragment readily trap an additional metal atom leading to the linearly ordered and the A-frame trinuclear structures, respectively. The arrangements, *syn* and *anti*, of the two pendant-arm phosphine units in the dimers may play a critical role in determining the

**Scheme 6**

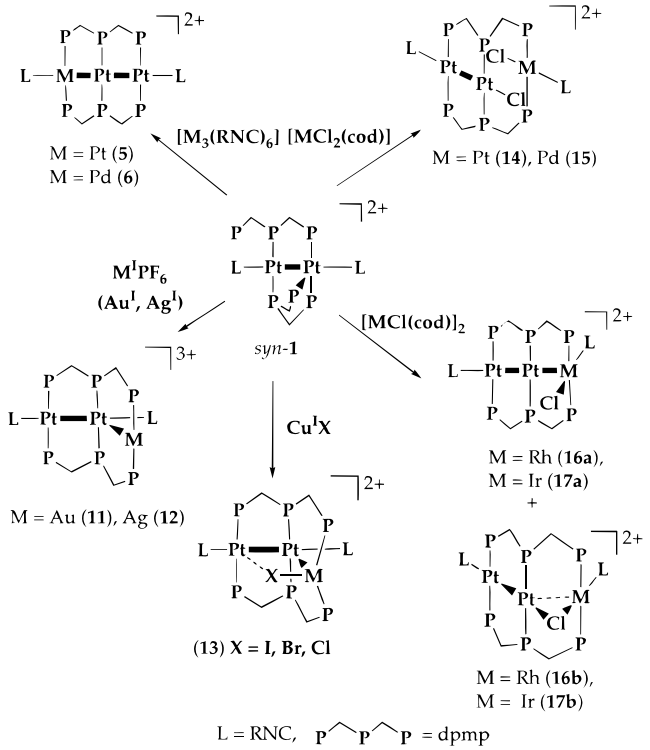

direction of $d^{10}$ metal-inserted position; the additional metal is incorporated into the terminal site of the trinuclear core from the *syn*-dimer and into the central position from the *anti*-dimer. In particular, the side-by-side type linearly ordered trinuclear clusters **5** and **6** having 44 valence electrons are of general interest as mimetic models for the interactions of the surfaces of heterogeneous catalysts with small molecules. Further, the synthetic methodology to produce Pt−Pt−M heterotrinuclear clusters from the *syn*-dimer is interestingly contrasted to those reactions by using dinuclear complexes of dpma (bis((diphenylphosphino)methyl)-phenylarsine) and $(Ph_2P)_2py$ (2,6-bis(diphenylphosphino)pyridine) which can house a heteroatom in the middle position,[4,32] and may thus lead to a new class of heterotrimetallic systems. In fact, the *syn*-dimer **1** has recently exhibited remarkable reactivity toward metal species to afford versatile heterotrinuclear complexes (Scheme 6). The reaction with $d^{10}$ Au(I) and Ag(I) ions gave the Y-shaped trinuclear complexes $[Pt_2M(\mu\text{-dpmp})_2(RNC)_2]^{3+}$ (M = Au, **11**; M = Ag, **12**)[33] and that with CuX produced $[Pt_2CuX(\mu\text{-dpmp})_2(RNC)_2]^{2+}$ (**13**),[33] while the reaction with $d^8$ $[MCl_2(cod)]$ (M = Pt, Pd) afforded the dimer−monomer-combined complexes $[Pt_2Cl\{MCl(RNC)\}(\mu\text{-dpmp})_2(RNC)]^{2+}$ (M = Pt, **14**; M = Pd, **15**).[27] The similar treatment with $d^8$ $[MCl(cod)]_2$ (M = Rh, Ir) led to formation of the Pt−Pt−M T-shaped clusters, $[Pt_2\{MCl(RNC)\}(\mu\text{-dpmp})_2(RNC)]^{2+}$ (M = Rh, **16a**; M = Ir, **17a**), which involve a M→Pt dative bond, and the Pt−Pt−M A-frame complexes, $[Pt_2(\mu\text{-Cl})M(\mu\text{-dpmp})_2(RNC)_2]^{2+}$ (M = Rh, **16b**; M = Ir, **17b**).[34] This family of homo- and heterotrinuclear complexes could provide a useful platform to explore new catalytic reactions.

**Acknowledgment.** This work was partially supported by a Grant-in-Aid for Scientific Research from the Ministry of Education of Japan.

**Supporting Information Available:** Tabulations of crystallographic data, positional and thermal parameters, and bond lengths and angles for all non-hydrogen atoms for **1a**, **2a**, and **3**−**8** (71 pages). Ordering information is given on any current masthead page.

OM970724S

(32) Balch, A. L. *Pure Appl. Chem.* **1988**, *60*, 555.

(33) Tanase, T.; Toda, H.; Yamamoto, Y. *Inorg. Chem.* **1997**, *36*, 1571.

(34) Tanase, T.; Toda, H.; Kobayashi, K.; Yamamoto, Y. *Organometallics* **1996**, *15*, 5272.